but also on the degree of liver dysfunction (de Lope et al. 2012; Izumi et al. 1994).

The Child-Pugh (C-P) classification, also known as the Child-Turcotte-Pugh score, is commonly used to evaluate liver function in the context of chronic liver disease, mainly cirrhosis (Pugh et al. 1973). The C-P score is based on 5 factors, which are each assigned 1–3 points: serum bilirubin and serum albumin levels, prothrombin time, ascites, and encephalopathy. The total number of points can range from 5 to 15. In multivariate analysis, the C-P class is associated with mortality in liver cirrhosis patients (Merkel et al. 2000; Fernández-Esparrach et al. 2001).

The percentage of patients who had C-P class A liver function at the initial diagnosis of HCC is increasing in Japan (Toyoda et al. 2011) because of the development of surveillance systems for HCC. In addition, the increase in the average age of HCC patients results in the increase of HCC patients with C-P class A; HCC is likely to develop without the progressed liver disease in elderly patients (Umemura et al. 2009; Kumada et al. 2013a).

Furthermore, the treatment for viral hepatitis has been undergoing rapid change. All-oral drug combination therapy will be replaced by peginterferon and ribavirin in the near future in patients with chronic hepatitis C, which will achieve the eradication of HCV sustained virological response (SVR) (Lok et al. 2012; Afdhal et al. 2014a, b; Jacobson et al. 2013).

On the other hand, peginterferon and nucleos(t)ide analogue therapy has been reported to improve liver function among HBV-related chronic hepatitis and cirrhosis patients (Buster et al. 2007; Kumada et al. 2013b; Schiff et al. 2008; Shim et al. 2010).

With these progresses in treatments and managements of viral hepatitis, the number of HCC patients with C-P class A will be expected to increase.

Given the expected increase in the number of patients with C-P class A liver function at the diagnosis of HCC, it will be necessary to further discriminate the prognosis of HCC patients with C-P class A from the aspect of liver function. In the present study, we attempted to incorporate the liver fibrosis factors for the evaluation of the prognosis of HCC patients with C-P class A.

Several noninvasive biomarkers of liver fibrosis that may replace liver biopsy in the diagnosis of fibrosis have been reported (Leroy et al. 2007; Wai et al. 2003; Sebastiani et al. 2006). The FIB-4 index is a noninvasive liver fibrosis evaluation method calculated by using age, aspartate aminotransferase (AST), alanine aminotransferase (ALT), and platelet count is one noninvasive liver fibrosis evaluation method. Vallet-Pichard et al. (2007) reported that the FIB-4 index is concordant with FibroTest results.

The aim of this study was to assess the utility of the FIB-4 index in assessing the prognosis of HCC patients with C-P class A.

Methods

Patients and HCC follow-up protocol

Between 1992 and 2012, a total of consecutive 1,340 patients were diagnosed with HCC at the Department of Gastroenterology of Ogaki Municipal Hospital, Japan. Patients with C-P class B ($n = 334$) and C ($n = 91$) were excluded from this analysis. Therefore, we investigated 915 HCC patients with C-P class A disease in the present study.

HCC was diagnosed on the basis of histological examination of tumor tissue in 423 patients (46.2 %) including 401 patients who underwent hepatectomy and 22 patients who underwent percutaneous liver biopsy. In the remaining 492 patients, the diagnosis was confirmed by typical radiological findings according to the guidelines of the European Association for the Study of the Liver (EASL) guidelines (2012).

All laboratory data were measured at the time of HCC diagnosis, including tumor markers for HCC [i.e., α-fetoprotein (AFP), *Lens culinaris* agglutinin-reactive α-fetoprotein (AFP-L3), des-γ-carboxy prothrombin (DCP)].

All patients received regular follow-up examinations at three-month intervals at our institution, which consisted of imaging studies, either ultrasonography (US), contrast-enhanced computed tomography (CT), or magnetic resonance imaging (MRI), and measurement of HCC tumor markers. We selected the treatment strategies for HCC according to the clinical practice guidelines of the Japan Society of Hepatology (2009). The study protocol was approved by the institutional review board and was conducted in compliance with the Helsinki Declaration.

Calculation of the FIB-4 index

The FIB-4 index was calculated at the time of HCC diagnosis using the following formula: FIB-4 index = AST [IU/L] × age [years]/platelet count [10^9/L] × ALT [IU/L]$^{1/2}$. The optimal FIB-4 index cutoff point was determined using a Cox proportional hazards model and the distribution of patients. Patients were grouped according to their FIB-4 index score as follows: <2.0 ($n = 93$), ≥2.0 and <4.0 ($n = 311$), and ≥4.0 ($n = 511$). Patients with a C-P score 5 and 6 were grouped according to their FIB-4 index score as follows: <2.0 ($n = 79$ and 14, respectively), ≥2.0 and <4.0 ($n = 245$ and 66, respectively), and ≥4.0

($n = 282$ and 229, respectively). Patients who underwent hepatectomy/locoregional ablative therapy [LAT, which included radiofrequency ablation (RFA) and ethanol injection] were grouped according to their FIB-4 index score as follows: <2.0 ($n = 70$), ≥2.0 and <4.0 ($n = 222$), and ≥4.0 ($n = 357$).

Statistical analysis

The SPSS software package, version 15.0 (SPSS Inc, Chicago, IL, USA) was used for statistical analysis. Continuous variables are expressed as medians (first quartile–third quartile points). An actuarial analysis of the cumulative survival and recurrence rates was performed using the Kaplan–Meier method, and differences across groups were compared using the log-rank test. Cox proportional hazards modeling with forward selection was used to estimate the hazard ratios (HRs) for the survival rate associated with the following parameters: etiology (viral or non-viral hepatitis), C-P score (5 or 6 points), AFP (≤20 or >20 ng/mL), AFP-L3 (≤10 or >10 %), DCP (≤40 or >40 mAU/mL), FIB-4 index (<2.0, ≥2.0 and <4.0, or ≥4.0), tumor size (<3 or ≥3 cm), number of tumors (single or multiple), vascular invasion (absent or present), and hepatectomy as initial treatment for HCC. We used the lower or upper limit of the reference values at our institute as cutoff values for laboratory data. Statistical significance was defined as $p < 0.05$.

Results

Patient characteristics

The characteristics of the study patients are shown in Table 1. The median age was 69 years, and there was a predominance of men (73.3 %). The majority of patients were infected with HCV (69.9 %). HBV infection was observed in 15.6 % of patients. Alcohol abuse was defined as ≥60 g/day intake. One hundred and fifteen patients with HCV infection underwent interferon (IFN)-based antiviral therapy. Of these, 30 patients (21.6 %) achieved sustained virological response (SVR). SVR was defined by the absence of serum HCV RNA 24 weeks after the end of the treatment. Of 153 patients with HBV infection, 89 (58.2 %) received nucleos(t)ide analogue therapy.

There were 606 (66.2 %) patients with C-P score of 5 and 309 (33.8 %) with C-P score of 6. The median of FIB-4 of whole patients' index was 4.4. It was 3.7 in patients with C-P score 5, and 6.3 in those with C-P score 6, respectively. The median follow-up period was 3.0 years. Of the 915 patients, 401 underwent hepatectomy, 248 were treated with LAT, and 170 were initially treated with transcatheter arterial chemoembolization (TACE).

Overall survival rate of entire patients based on Child-Pugh score

The overall survival rates of entire patients at 5 and 10 years were 52.7 % [95 % confidence interval (CI) 48.8–56.2] and 29.7 % (95 % CI 25.7–34.1), respectively (Fig. 1). The overall survival rate for patients with C-P score 5 was 60.5 % (95 % CI 55.7–64.5) at 5 years and 33.9 % (95 % CI 28.9–39.3) at 10 years, compared to 36.3 % (95 % CI 30.1–42.9) at 5 years and 20.8 % (95 % CI 14.4–29.0) at 10 years in patients with C-P score 6. The group with C-P score 5 had a significantly better prognosis than the group with C-P score 6 ($p < 0.001$) (Fig. 2).

Table 1 Clinical background of the study patients ($n = 915$)

Age (years)	69 (62–75)
Sex (female/male)	244 (26.7 %)/671 (73.3 %)
Etiology (HBV/HCV/HBV + HCV/non-HBV and non-HCV)	143 (15.6 %)/640 (69.9 %)/10 (1.1 %)/122 (13.3 %)
Alcohol abuse (negative/positive)	666 (72.8 %)/249 (27.2 %)
Ascites (absent/present)	902 (98.6 %)/13 (1.4 %)
Encephalopathy (absent/present)	909 (99.3 %)/6 (0.7 %)
AST (IU/mL)	53 (36–79)
ALT (IU/mL)	45 (28–73)
Platelet count ($\times 10^4/m^3$)	12.6 (9.0–17.4)
Prothrombin time (%)	90 (88–99)
Total bilirubin (mg/dL)	0.7 (0.5–1.0)
Albumin (g/dL)	3.8 (3.5–4.1)
Child-Pugh score (5/6)	606 (66.2 %)/309 (33.8 %)
AFP (ng/mL)	19 (6–144)
AFP-L3 (%)	0.5 (0–11.6)
DCP (mAU/mL)	49 (20–389)
FIB-4 index	4.4 (2.8–6.8)
Tumor size (cm)	2.5 (1.7–4.3)
Tumor number (single/multiple)	570 (62.3 %)/345 (37.7 %)
Vascular invasion (absent/present)	801 (87.5 %)/114 (12.5 %)
Initial treatment	
No treatment/hepatectomy/LAT	48 (5.2 %)/401(43.8 %)/248 (27.1 %)
TACE/other[a]	170 (18.6 %)/48 (5.2 %)
Observation period (years)	3.0 (1.3–5.7)

Values are expressed as medians (first quartile, third quartile points)

HBV hepatitis B virus, *HCV* hepatitis C virus, *AST* aspartate aminotransferase, *ALT* alanine aminotransferase, *AFP* α-fetoprotein, *AFP-L3 Lens culinaris* agglutinin-reactive α-fetoprotein, *DCP* des-γ-carboxy prothrombin, *LAT* locoregional ablative therapy, *TACE* transcatheter arterial chemoembolization

[a] Includes repeated arterial infusion chemotherapy, systemic chemotherapy, and radiation therapy

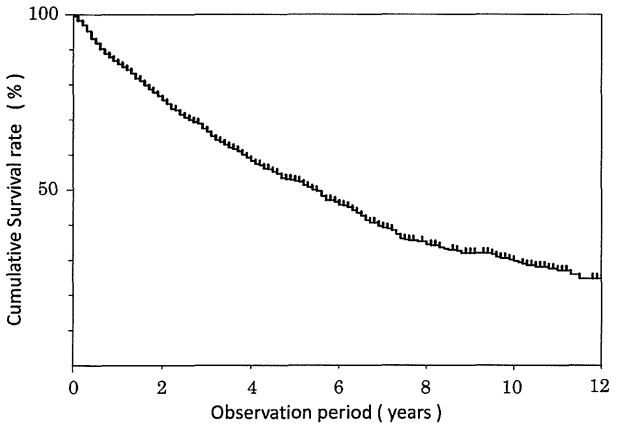

Fig. 1 Overall survival rates of entire patients at 5 and 10 years were 52.7 and 29.7 %, respectively

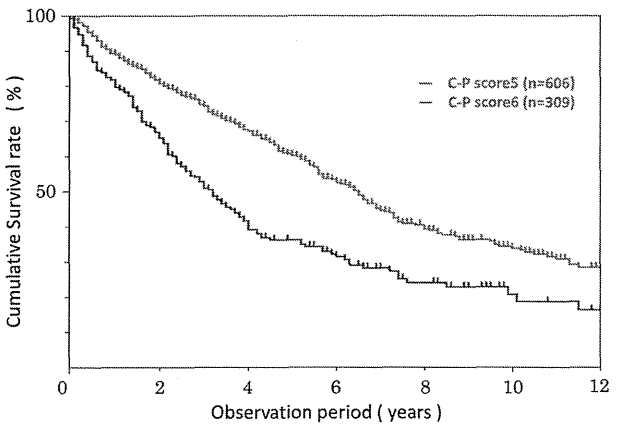

Fig. 2 Prognosis of the Child-Pugh score 5 group was significantly better compared to the Child-Pugh score 6 group

Overall survival rate of entire patient based on the FIB-4 index

When patients were categorized according to the FIB-4 index as <2.0 ($n = 93$), ≥2.0 and <4.0 ($n = 311$), and ≥4.0 ($n = 511$), the survival rates at were 70.5 % (95 % CI 59.0–79.9), 56.4 % (95 % CI 50.1–62.5), and 47.1 % (95 % CI 42.2–52.1) at 5 years, respectively, and 55.3 % (95 % CI 42.2–67.7), 32.2 % (95 % CI 25.5–39.6), and 23.7 % (95 % CI 18.6–29.7) at 10 years, respectively (Fig. 3). The FIB-4 index <2.0 group had a significantly better prognosis than the FIB-4 index ≥2.0 and <4.0 group ($p = 0.028$). The FIB-4 index ≥2.0 and <4.0 group had a significantly better prognosis than the FIB-4 index ≥4.0 group ($p = 0.010$).

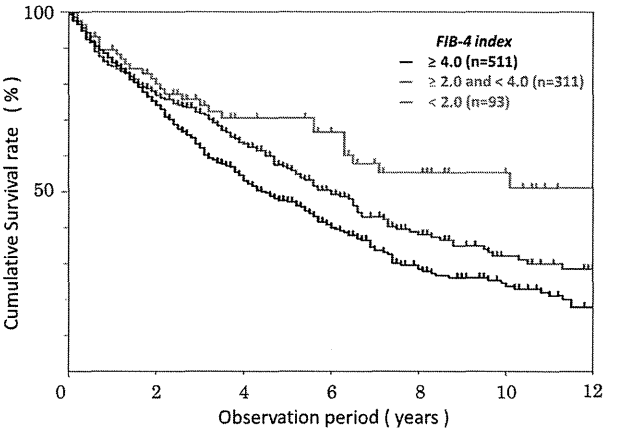

Fig. 3 Overall survival rate based on the FIB-4 index. The FIB-4 index of patients with Child-Pugh class A predicts outcomes with good discriminative ability

Overall survival and recurrence rate of patients who underwent hepatectomy/LAT based on the FIB-4 index

When focusing on HCC patients who underwent hepatectomy/LAT, FIB-4 index was <2.0 in 70 patients (10.8 %), ≥2.0 and <4.0 in 222 patients (34.2 %), and ≥4.0 in 357 patients (55.0 %). Figure 4a shows the overall survival rates of these three groups. The survival rates of the FIB-4 index <2.0, ≥2.0 and <4.0, and ≥4.0 groups were 80.0 % (95 % CI 67.1–88.7), 68.9 % (95 % CI 61.7–75.2), and 59.1 % (95 % CI 53.2–64.7) at 5 years, respectively, and 65.2 % (95 % CI 49.4–78.1), 40.9 % (95 % CI 32.6–49.9), and 28.6 % (95 % CI 22.1–36.1) at 10 years, respectively. The FIB-4 index <2.0 group had a significantly better prognosis than the FIB-4 index ≥2.0 and <4.0 group ($p = 0.047$). The FIB-4 index ≥2.0 and <4.0 group had a significantly better prognosis than the FIB-4 index ≥4.0 group ($p = 0.005$).

Figure 4b shows overall intrahepatic recurrence rates following the initial treatment in these three groups. The recurrence rates of patients with FIB-4 index <2.0, ≥2.0 and <4.0, and ≥4.0 were 54.3 % (95 % CI 52.4–79.5), 63.6 % (95 % CI 56.1–70.5) and 79.6 % (95 % CI 74.5–89.0), respectively, at 5 years and 67.4 % (95 % CI 52.4–79.5), 79.0 % (95 % CI 70.6–85.5) and 89.7 % (95 % CI 84.2–93.4), respectively, at 10 years. The FIB-4 index ≥4.0 group had a significantly higher recurrence rate than the other groups (FIB-4 index ≥4.0 vs ≥2.0 and <4.0, $p < 0.001$; ≥4.0 vs <2.0, $p = 0.001$). There were no significant differences in recurrence rate between the FIB-4 index <2.0 and ≥2.0 and <4.0 groups ($p = 0.465$).

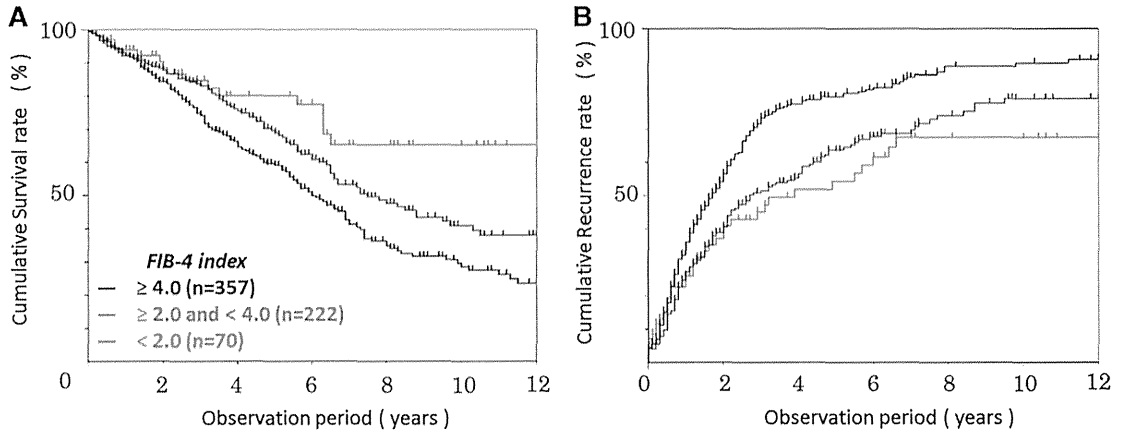

Fig. 4 Overall survival (**a**) and recurrence rate (**b**) based on the FIB-4 index in patients who underwent hepatectomy/LAT. The FIB-4 index <2.0 group had a significantly better prognosis than the other groups, and the recurrence rate of FIB-4 index ≥4.0 group was higher than that of the other groups

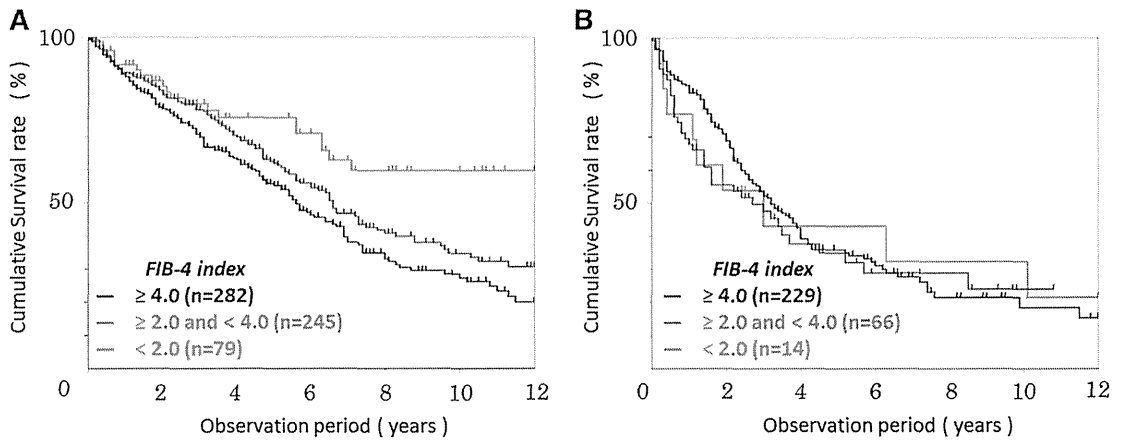

Fig. 5 Overall survival rates of patients with a Child-Pugh score of 5 (**a**) and 6 (**b**) based on the FIB-4 index. The FIB-4 index was useful for assessing mortality among patients with a Child-Pugh score of 5, but there were no significant difference among patients with a Child-Pugh score of 6

Overall survival rate of patients with C-P score 5 or 6 based on the FIB-4 index

When focusing on HCC patients with C-P score 5, FIB-4 index was <2.0 in 79 patients (13.0 %), ≥2.0 and <4.0 in 245 patients (40.4 %), and ≥4.0 in 282 patients (46.5 %). Figure 5a shows the overall survival rates of these three groups. The survival rates of the FIB-4 index <2.0, ≥2.0 and <4.0, and ≥4.0 groups were 75.7 % (95 % CI 63.2–84.9), 61.9 % (95 % CI 54.8–68.5), and 55.2 % (95 % CI 48.6–61.5) at 5 years, respectively, and 59.7 % (95 % CI 44.9–72.9), 34.7 % (95 % CI 27.1–43.2), and 27.3 % (95 % CI 20.6–35.3) at 10 years, respectively. The survival rate was highest in patients with FIB-4 index <2.0, followed by those with FIB-4 index ≥2.0 and <4.0, and those with FIB-4 index ≥4.0, although the difference between patients with FIB-4 index ≥2.0 and <4.0 and those with FIB-4 index ≥4.0 was not significant statistically (FIB-4 index <2.0 vs ≥2.0 and <4.0, $p = 0.028$, FIB-4 index <2.0 vs ≥4.0, $p < 0.001$, and FIB-4 index ≥2.0 and <4.0 vs ≥4.0, $p = 0.052$).

When focusing on HCC patients with C-P score 6, FIB-4 index was <2.0 in 14 patients (4.5 %), ≥2.0 and <4.0 in 66 patients (21.4 %), and ≥4.0 in 229 patients (74.1 %). Figure 5b shows overall survival rate of these three groups. The survival rate of patients with FIB-4 index <2.0, ≥2.0 and <4.0, and ≥4.0 were 43.1 % (95 % CI 19.0–71.0), 35.0 % (95 % CI 22.9–49.4) and 36.0 % (95 % CI 28.8–43.8), respectively, at 5 years and 32.3 % (95 % CI 11.6–63.5), 24.1 % (95 % CI 12.7–40.8) and 18.4 % (95 % CI

Table 2 Factors associated with patient survival (univariate analysis)

Factor	Hazard ratio	95 % CI	*p* value
Age (years)			
<65	1		
≥65	1.335	1.095–1.628	0.004
Sex			
Female	1		
Male	1.156	0.605–1.422	0.172
AST (IU/mL)			
≤40	1		
>40	1.518	1.235–1.860	0.001
ALT (IU/mL)			
≤35	1		
>35	1.158	0.954–1.407	0.139
Platelet count ($\times 10^4/m^3$)			
≥15	1		
<15	1.026	0.804–1.181	0.792
Total bilirubin (mg/dL)			
≤1.2	1		
>1.2	1.195	0.888–1.608	0.239
Albumin (g/dL)			
>3.5	1		
≤3.5	1.912	1.549–2.360	<0.001
Prothrombin time (%)			
>70	1		
≤70	1.086	0.519–1.634	0.921
Etiology (viral hepatitis)			
Present	1		
Absent	1.356	1.041–1.761	0.024
Child-Pugh score			
5	1		
6	1.845	1.528–2.227	<0.001
Alcohol abuse			
Absent	1		
Present	1.033	0.844-1.264	0.756
AFP (ng/mL)			
≤20	1		
>20	1.449	1.207–1.739	<0.001
AFP-L3 (%)			
≤10	1		
>10	1.904	1.549–2.342	<0.001
DCP (mAU/mL)			
≤40	1		
>40	1.614	1.339–1.945	<0.001
FIB-4 index			
<2.0	1		
≥2.0 and <4.0	1.550	1.048–2.292	0.028
≥4.0	2.001	5.761–2.917	<0.001
Tumor size (cm)			
<3	1		
≥3	2.220	1.849–2.665	<0.001
Tumor number			
Single	1		
Multiple	2.350	1.953–2.824	<0.001
Vascular invasion			
Absent	1		
Present	4.989	3.883–6.410	<0.001
Antiviral therapy			
−	1		
+	0.501	0.393–0.639	<0.001
Initial treatment			
Hepatectomy			
−	1		
+	0.438	0.368–0.531	<0.001
LAT			
−	1		
+	0.880	0.717–1.071	0.218

CI confidence interval, *AST* aspartate aminotransferase, *ALT* alanine aminotransferase, *AFP* α-fetoprotein, *AFP-L3 Lens culinaris* agglutinin-reactive α-fetoprotein, *DCP* des-γ-carboxy prothrombin, *LAT* locoregional ablative therapy

11.1–28.9), respectively, at 10 years. There were no significant differences in survival rates among these three groups (FIB-4 index <2.0 vs ≥2.0 and <4.0, $p = 0.812$; FIB-4 index <2.0 vs ≥4.0, $p = 0.743$; FIB-4 index ≥2.0 and <4.0 vs ≥4.0, $p = 0.393$).

Factors associated with patient survival

Factors significantly associated with overall survival in the univariate analysis are listed in Table 2. The following associations were statistically significant: age, AST, albumin, HCC etiology, C-P score, AFP, AFP-L3, DCP, FIB-4 index, tumor size, number of tumors, vascular invasion, antiviral therapy, and hepatectomy/LAT as initial treatment. Factors that were significantly associated with overall survival in the multivariate analysis were C-P score 6 [HR 1.564 (95 % CI 1.257–1.946); $p < 0.001$], FIB-4 index ≥2.0 and <4.0 [HR 1.638 (95 % CI 1.084–2.474); $p = 0.019$] and FIB-4 index ≥4.0 [HR 1.828 (95 % CI 1.217–2.744); $p = 0.004$], AFP-L3 >10 % [HR 1.458 (95 % CI 1.163–1.829); $p = 0.001$], tumor size ≥3 cm [HR 1.718 (95 % CI 1.382–2.136); $p < 0.001$], number of tumors (multiple) [HR 1.464 (95 % CI 1.172–1.828); $p = 0.001$], vascular invasion (present) [HR 2.884 (95 % CI 2.102–3.957); $p < 0.001$], antiviral therapy [HR 0.761 (95 % CI 0.585–0.989); $p = 0.041$], and hepatectomy as initial treatment [HR 0.625 (95 % CI 0.497–0.786); $p < 0.001$] (Table 3).

Table 3 Factors associated with patient survival based on multivariable Cox proportional hazards modeling with forward selection

Factor	Hazard ratio	95 % CI	*p* value
Child-Pugh score			
5	1		
6	1.564	1.257–1.946	<0.001
FIB-4 index			
<2.0	1		
≥2.0 and <4.0	1.638	1.084–2.474	0.019
≥4.0	1.828	1.217–2.744	0.004
AFP-L3 (%)			
≤10	1		
>10	1.458	1.163–1.829	0.001
Tumor size (cm)			
<3	1		
≥3	1.718	1.382–2.136	<0.001
Tumor number			
Single	1		
Multiple	1.464	1.172–1.828	0.001
Vascular invasion			
Absent	1		
Present	2.884	2.102–3.957	<0.001
Antiviral therapy			
−	1		
+	0.761	0.585–0.989	0.041
Initial treatment			
Hepatectomy			
−	1		
+	0.625	0.497–0.786	<0.001

CI confidence interval, *AFP-L3 Lens culinaris* agglutinin-reactive α-fetoprotein

Discussion

C-P classification and tumor staging are both important factors for predicting mortality in HCC patients. Therefore, we have to assess both tumor factors and residual liver function when choosing the type of treatment for HCC. Recently, proposed staging system for HCC combined tumor factors and liver functional markers has been reported (the Cancer of the Liver Italian Program (CLIP) investigators 1998; Llovet et al. 1999; Kudo et al. 2004).

In patients with HCC who have C-P class A liver function at diagnosis, in the present study, there were significant differences in the survival rates between C-P score 5 and 6 groups. However, we are not able to further stratify HCC patients with C-P score 5 in terms of liver function, because the minimum score of C-P is 5 points.

It has been reported that the FIB-4 index is well correlated with liver fibrosis (Sterling et al. 2006; Vallet-Pichard et al. 2007; Shah et al. 2009). Although liver fibrosis is reportedly intertwined with hepatocarcinogenesis and the prognosis of chronic hepatitis C (Tamaki et al. 2013; Vergniol et al. 2014), there have been few reports on whether the FIB-4 index is associated with mortality in HCC patients. In this study, we investigated the impact of the FIB-4 index on prognosis of HCC with C-P class A.

When patients were categorized as <2.0, ≥2.0 and <4.0, and ≥4.0 by FIB-4 index, patients with FIB-4 index <2.0 had a highest survival rate, followed by those with FIB-4 index ≥2.0 and <4.0, and those with FIB-4 index ≥4.0. In addition, the FIB-4 index was also useful for predicting prognosis in patients who underwent curative treatment (hepatectomy/LAT), and the recurrence rate of FIB-4 index ≥4.0 group was higher than that of the other groups in this analysis. These results indicate that the calculation of the FIB-4 index at the start of follow-up is useful for predicting the outcome of HCC patients with C-P class A.

Whereas we found a significant difference in survival rates based on the FIB-4 index in patients with C-P score 5, we did not find a difference in survival rates in patients with C-P score 6. The C-P scoring system is considered to reflect remnant liver function. In contrast, the FIB-4 index is a marker of liver fibrosis. Although liver fibrosis is partly linked to remnant liver function, these are not completely coincident. Patients with C-P class A can have various degrees of liver fibrosis. Therefore, we were able to further stratify the prognosis of HCC patients with C-P score 5 using the FIB-4 index, a quantitative marker of liver fibrosis.

Both the FIB-4 index and C-P score were identified as independent risk factors for predicting the outcome of HCC along with tumor factors such as tumor size, number, and tumor marker levels, and initial treatment in the multivariate analysis. In addition, the hazard ratio of the FIB-4 index was higher than the HR for the C-P score. Therefore, FIB-4 index has a strong impact on the prognosis of patients with HCC when they have C-P class A liver function.

The utility of FIB-4 index is enhanced by the fact that it is calculated using age and general laboratory data, in terms of low cost, easy to calculate. In addition, the index can be monitored easily with repeated calculation. Nevertheless, the FIB-4 index has several limitations. The formula for the FIB-4 index includes platelet count. Therefore, caution is needed when a patient's platelet count is low due to extrahepatic causes, for example, idiopathic thrombocytopenic purpura and post-splenectomy.

There are several issues that should be further studied in the future. The FIB-4 index has been developed as a noninvasive marker of fibrosis in patients with chronic hepatitis C and non-alcoholic fatty liver disease (Sterling et al. 2006; Vallet-Pichard et al. 2007; Shah et al. 2009). Since the predominant etiology of HCC in the present study was HCV,

further studies are required for assessing the prognosis of HCC due to other etiologies (HBV and non-HBV + HCV). Additionally, we did not investigate other serum liver fibrosis markers including hyaluronic acid and type IV collagen 7s. Hence, it is necessary to assess the utility of these values for the prediction of prognosis in HCC patients and their relationship to the FIB-4.

In conclusion, the FIB-4 index was closely associated with mortality in HCC patients with C-P class A, especially those with C-P score 5. The FIB-4 index was identified as an independent predictive factor for HCC prognosis from a set of tumor and therapy-related factors. Therefore, the FIB-4 index is very useful to clinicians when predicting mortality and determining treatment strategies for HCC patients with C-P score 5.

Acknowledgments There is no grant or other financial support for this study.

Conflict of interest The authors declare no conflicts of interests.

References

A new prognostic system for hepatocellular carcinoma (1998) A retrospective study of 435 patients: the Cancer of the Liver Italian Program (CLIP) investigators. Hepatology 28:751–755

Afdhal N, Zeuzem S, Kwo P, Chojkier M, Gitlin N, Puoti M et al (2014a) The ION-1 investigators. Ledipasvir and sofosbuvir for untreated HCV genotype 1 infection. N Engl J Med 370:1889–1898

Afdhal N, Reddy KR, Nelson DR, Lawitz E, Gordon SC, Schiff E et al (2014b) Ledipasvir and sofosbuvir for previously treated HCV genotype 1 infection. ION-2 investigators. N Engl J Med 370:1483–1493

Buster EH, Hansen BE, Buti M, Delwaide J, Niederau C, Michielsen PP et al (2007) HBV 99-01 Study Group. Peginterferon alpha-2b is safe and effective in HBeAg-positive chronic hepatitis B patients with advanced fibrosis. Hepatology 46:388–394

Clinical Practice Guidelines for Hepatocellular Carcinoma (2009) The Japan Society of Hepatology update. Hepatol Res 2010(40):2–144

de Lope CR, Tremosini S, Forner A, Reig M, Bruix J (2012) Management of HCC. J Hepatol 56:75–87

El-Serag HB, Rudolph KL (2007) Hepatocellular carcinoma: epidemiology and molecular carcinogenesis. Gastroenterology 132:2557–2576

European Association for the Study of the Liver (2012) European Organisation for Research and Treatment of Cancer. EASL-EORTC clinical practice guidelines: management of hepatocellular carcinoma. J Hepatol 56:908–943

Fernández-Esparrach G, Sánchez-Fueyo A, Ginès P, Uriz J, Quintó L, Ventura PJ et al (2001) A prognostic model for predicting survival in cirrhosis with ascites. J Hepatol 34:46–52

Izumi R, Shimizu K, Ii T, Yagi M, Matsui O, Nonomura A et al (1994) Prognostic factors of hepatocellular carcinoma in patients undergoing hepatic resection. Gastroenterology 106:720–727

Jacobson IM, Gordon SC, Kowdley KV, Yoshida EM, Rodriguez-Torres M, Sulkowski MS et al (2013) POSITRON Study; FUSION Study; Sofosbuvir for hepatitis C genotype 2 or 3 in patients without treatment options. N Engl J Med 368:1867–1877

Jemal A, Bray F, Center MM, Ferlay J, Ward E, Forman D (2011) Global cancer statistics. CA Cancer J Clin 61:69–90

Kudo M, Chung H, Haji S, Osaki Y, Oka H, Seki T et al (2004) Validation of a new prognostic staging system for hepatocellular carcinoma: the JIS score compared with the CLIP score. Hepatology 40:1396–1405

Kumada T, Toyoda H, Kiriyama S, Tanikawa M, Hisanaga Y, Kanamori A et al (2013a) Characteristics of elderly hepatitis C virus-associated hepatocellular carcinoma patients. J Gastroenterol Hepatol 28:357–364

Kumada T, Toyoda H, Tada T, Kiriyama S, Tanikawa M, Hisanaga Y et al (2013b) Effect of nucleos(t)ide analogue therapy on hepatocarcinogenesis in chronic hepatitis B patients: a propensity score analysis. J Hepatol 58:427–433

Leroy V, Hilleret MN, Sturm N, Trocme C, Renversez JC, Faure P et al (2007) Prospective comparison of six non-invasive scores for the diagnosis of liver fibrosis in chronic hepatitis C. J Hepatol 46:775–782

Llovet JM, Brú C, Bruix J (1999) Prognosis of hepatocellular carcinoma: the BCLC staging classification. Semin Liver Dis 19:329–338

Lok AS, Gardiner DF, Lawitz E, Martorell C, Everson GT, Ghalib R, Reindollar R, Rustgi V, McPhee F, Wind-Rotolo M, Persson A, Zhu K, Dimitrova DI, Eley T, Guo T, Grasela DM, Pasquinelli C et al (2012) Preliminary study of two antiviral agents for hepatitis C genotype 1. N Engl J Med 366:216–224

Merkel C, Bolognesi M, Sacerdoti D, Bombonato G, Bellini B, Bighin R et al (2000) The hemodynamic response to medical treatment of portal hypertension as a predictor of clinical effectiveness in the primary prophylaxis of variceal bleeding in cirrhosis. Hepatology 32:930–934

Pugh RN, Murray-Lyon IM, Dawson JL, Pietroni MC, Williams R (1973) Transection of the oesophagus for bleeding oesophageal varices. Br J Surg 60:646–649

Schiff E, Simsek H, Lee WM, Chao YC, Sette H Jr, Janssen HL et al (2008) Efficacy and safety of entecavir in patients with chronic hepatitis B and advanced hepatic fibrosis or cirrhosis. Am J Gastroenterol 103:2776–2783

Sebastiani G, Vario A, Guido M, Noventa F, Plebani M, Pistis R et al (2006) Stepwise combination algorithms of non-invasive markers to diagnose significant fibrosis in chronic hepatitis C. J Hepatol 44:686–693

Shah AG, Lydecker A, Murray K, Tetri BN, Contos MJ, Sanyal AJ (2009) Nash Clinical Research Network. Comparison of noninvasive markers of fibrosis in patients with nonalcoholic fatty liver disease. Clin Gastroenterol Hepatol 7:1104–1112

Shim JH, Lee HC, Kim KM, Lim YS, Chung YH, Lee YS et al (2010) Efficacy of entecavir in treatment-naïve patients with hepatitis B virus-related decompensated cirrhosis. J Hepatol 52:176–182

Sterling RK, Lissen E, Clumeck N, Sola R, Correa MC, Montaner J et al (2006) APRICOT Clinical Investigators. Development of a simple noninvasive index to predict significant fibrosis in patients with HIV/HCV coinfection. Hepatology 43:1317–1725

Tamaki N, Kurosaki M, Matsuda S, Muraoka M, Yasui Y, Suzuki S et al (2013) Non-invasive prediction of hepatocellular carcinoma development using serum fibrosis marker in chronic hepatitis C patients. J Gastroenterol. doi:10.1007/s00535-013-0914-y

Toyoda H, Kumada T, Tada T, Sone Y, Kaneoka Y, Maeda A (2011) Characteristics and prognosis of patients with hepatocellular carcinoma after the year 2000 in Japan. J Gastroenterol Hepatol 26:1765–1771

Umemura T, Ichijo T, Yoshizawa K, Tanaka E, Kiyosawa K (2009) Epidemiology of hepatocellular carcinoma in Japan. J Gastroenterol 44:102–107

Vallet-Pichard A, Mallet V, Nalpas B, Verkarre V, Nalpas A, Dhalluin-Venier V et al (2007) FIB-4: an inexpensive and accurate marker

of fibrosis in HCV infection. Comparison with liver biopsy and fibrotest. Hepatology 46:32–36

Vergniol J, Boursier J, Coutzac C, Bertrais S, Foucher J, Angel C et al (2014) The evolution of non-invasive tests of liver fibrosis is associated with prognosis in patients with chronic hepatitis C. Hepatology 60:65–76

Wai CT, Greenson JK, Fontana RJ, Kalbfleisch JD, Marrero JA, Conjeevaram HS et al (2003) A simple noninvasive index can predict both significant fibrosis and cirrhosis in patients with chronic heparins C. Hepatology 38:518–526

Archives of Biochemistry and Biophysics 565 (2015) 1–8

Contents lists available at ScienceDirect

Archives of Biochemistry and Biophysics

journal homepage: www.elsevier.com/locate/yabbi

Heat shock protein 20 (HSPB6) regulates TNF-α-induced intracellular signaling pathway in human hepatocellular carcinoma cells

Tomoaki Nagasawa [a], Rie Matsushima-Nishiwaki [a], Eisuke Yasuda [b,d], Junya Matsuura [a], Hidenori Toyoda [b], Yuji Kaneoka [c], Takashi Kumada [b], Osamu Kozawa [a,*]

[a] Department of Pharmacology, Gifu University Graduate School of Medicine, Gifu 501-1194, Japan
[b] Department of Gastroenterology, Ogaki Municipal Hospital, Ogaki, Gifu 503-8502, Japan
[c] Department of Surgery, Ogaki Municipal Hospital, Ogaki, Gifu 503-8502, Japan
[d] Department of Radiological Technology, Suzuka University of Medical Science, Suzuka 513-8670, Japan

ARTICLE INFO

Article history:
Received 15 July 2014
and in revised form 2 October 2014
Available online 27 October 2014

Keywords:
HSP20
TNF-α
HCC
IKK-α
Cell proliferation

ABSTRACT

We previously demonstrated that the expression of HSP20, a small heat shock protein, is inversely correlated with the progression of HCC. Inflammation is associated with HCC, and numerous cytokines, including TNF-α, act as key mediators in the progression of HCC. In the present study, we investigated whether HSP20 is implicated in the TNF-α-stimulated intracellular signaling in HCC using human HCC-derived HuH7 cells in the presence of TNF-α. In HSP20-overexpressing HCC cells, the cell growth was retarded compared with that in the control cells under long-term exposure of TNF-α. Because NF-κB pathway is the main intracellular signaling system activated by TNF-α, we investigated the effects of HSP20-overexpression of this pathway. The protein levels of IKK-α, but not IKK-β, in the HSP20-overexpressing cells were decreased. Short-term exposure to TNF-α-induced phosphorylation and degradation of IκB, and the phosphorylation and transactivational activity of NF-κB were suppressed in the HSP20-overexpressing HCC cells. Furthermore, the increase in IKK-α levels was accompanied by a decrease in the HSP20 levels in human HCC tissues. These findings strongly suggest that HSP20 might decrease the IKK-α protein level and that it down-regulates the TNF-α-stimulated intracellular signaling in HCC, thus resulting in the suppression of HCC progression.

Introduction

Human hepatocellular carcinoma (HCC),[1] a primary cancer of the liver, is a major cause of cancer-related death worldwide, especially in developing countries. Even after surgical resection, HCC recurs at a high frequency. The five-year survival rate of HCC is 30–40% [1]. HCC frequently develops as a consequence of underlying liver disease, which is accompanied with chronic inflammation. Inflammation occurs with chronic hepatitis or liver cirrhosis, and is thought to induce HCCs [1,2]. Proinflammatory cytokines, including tumor necrosis factor-α (TNF-α), are implicated in the pathogenesis of HCC [2]. In the liver, it has been shown that TNF-α stimulates hepatocyte proliferation, in addition to acting as a mediator of cell death [2,3]. Regarding the intracellular signaling of TNF-α, it is generally established that the nuclear factor-κB (NF-κB) pathway is the main signaling system [3]. TNF-α stimulates the activation of inhibitor κB kinase (IKK) and consequently induces the transcriptional activities of NF-κB via the phosphorylation and subsequent degradation of inhibitor κB (IκB) proteins [3]. Once IκB is phosphorylated, it releases NF-κB, thus resulting in its translocation to the nucleus, where it regulates transcriptional events.

It has been shown that NF-κB signaling is critically involved in the progression of HCC [2,3]. The inhibition of the NF-κB activity at later stages of carcinogenesis reportedly reduces inflammation-associated tumor development in liver parenchymal cells [2]. In addition, TNF-α-activated NF-κB signaling promotes the expression of epidermal growth factor (EGF) receptor ligands, such as transforming growth factor-α (TGF-α), and stimulates their release from the cell surface, which enhances HCC cell survival and

* Corresponding author. Fax: +81 58 230 6215.
E-mail address: okozawa@gifu-u.ac.jp (O. Kozawa).

[1] *Abbreviations used:* HCC, human hepatocellular carcinoma; TNF-α, tumor necrosis factor-α; NF-κB, nuclear factor-κB; IKK, inhibitor κB kinase; IκB, inhibitor κB; EGF, epidermal growth factor; TGF-α, transforming growth factor-α; HSF, heat shock factor; UICC, Union of International Cancer Control; MAPK, mitogen-activated protein kinase; PI3K, phosphoinositide 3-kinase; GAPDH, glyceraldehyde-3-phosphate dehydrogenase; RPMI, Roswell Park Memorial Institute; FCS, fetal calf serum; SDS, sodium dodecyl sulfate; PAGE, polyacrylamide gel electrophoresis; PVDF, polyvinylidene fluoride; PBS, phosphate-buffered saline; DHMEQ, dehydroxymethylepoxyquinomicin.

http://dx.doi.org/10.1016/j.abb.2014.10.010
0003-9861/

proliferation [2]. However, the regulatory mechanism underlying the TNF-α-induced NF-κB signaling pathway in HCC has not yet been clarified.

Heat shock protein 20 (HSP20/HSPB6) belongs to the small HSP family (HSPB) with monomeric molecular masses ranging from 15 to 30 kDa. HSP20 is ubiquitously expressed in many organs, such as muscles and the liver [4–6]. The HSPB family has significant similarities in terms of amino acid sequences, so-called α-crystallin domain [6]. Although HSP20 has molecular chaperone activity, as well as other small HSPs, the expression of HSP20 is not induced by physical or chemical stresses, and does not seem to depend on the action of heat shock factor (HSF)-1 [6]. However, some physiological factors might affect HSP20 expression. Accumulating evidence suggests that HSP20 is implicated in multiple physiological and pathological processes, such as the regulation of smooth muscle relaxation, myocardial infarction and Alzheimer's disease [6–8]. In our previous studies [9,10], we have demonstrated that HSP20 functions extracellularly to suppress the aggregation and activation of human platelets. Regarding HSP20 in HCC, we have reported that the expression levels of HSP20 in human HCCs are inversely proportional to the TNM stage [11]. The TNM classification is a cancer staging system proposed and updated by the Union of International Cancer Control (UICC). It records the primary and regional nodal extent of the tumor and the absence or presence of metastasis. In addition, we showed that HSP20 reduces HCC cell growth by suppressing the mitogen-activated protein kinase (MAPK) and phosphoinositide 3-kinase (PI3K)/AKT pathways, which are stimulated by growth factors such as TGF-α [12,13]. HSP20 directly interacts with PI3K and inhibits the PI3K activity in HCCs [13]. Moreover, we recently showed that HSP20 directly interacts with Bax and regulates apoptosis in HCC cells [14].

In the present study, we investigated the involvement of HSP20 in the TNF-α-induced NF-κB signaling pathway in HCC cells. We herein demonstrate that HSP20 regulates IKK-α protein expression and suppresses the TNF-α-induced NF-κB signaling pathway in human HCC.

Materials and methods

Materials

TNF-α was obtained from Funakoshi Pharmaceutical Co. Ltd. (Tokyo, Japan). Wedelolactone was obtained from Calbiochem-Novabiochem, Co. (La Jolla, CA). HSP20 antibodies were purchased from Enzo Life Sciences Inc. (Farmingdale, NY). Antibodies against IKK-α, IKK-β, IκB, phospho-specific IκB, NF-κB p65 and phospho-specific NF-κB p65 (Ser-536) were purchased from Cell Signaling Technology, Inc. (Danvers, MA). Anti-HSP27 and anti-glyceraldehyde-3-phosphate dehydrogenase (GAPDH) antibodies were purchased from Santa Cruz Biotechnology Inc. (Santa Cruz, CA). Wild-type human HSP20 cDNA (clone ID 6074542), which was obtained from Open Biosystems, Inc. (Huntsville, AL), was subcloned into the eukaryotic expression vector, pcDNA 3.1(+), as described previously [12]. The eukaryotic expression vector, pcDNA 3.1(+), control short interfering RNA (siRNA) [Silencer Negative Control No.1 siRNA] and HSP20-siRNAs [Silencer® Select siRNA; s43029 (#29) and s43030 (#30)] and the Trizol reagent were purchased from Life Technologies Corp. (Carlsbad, CA). SiLentFect was purchased from Bio Rad (Hercules, CA). The Omniscript Reverse Transcriptase kit was purchased from QIAGEN (Hilden Germany). Fast-Start DNA Master SYBR green I was purchased from Roche Diagnostics (Mannheim, Germany). A reporter plasmid containing the luciferase reporter gene linked to five repeats of the NF-κB binding site, pNF-κB-luc, was obtained from Agilent Technologies Manufacturing GmbH & Co, (Waldbronn, Germany). The BCA protein assay kit was obtained from Thermo Fisher Scientific Inc. (Waltham, MA).

Cell cultures

Human HCC-derived HuH7 cells were obtained from the Health Science Research Resources Bank (Tokyo, Japan). The HuH7 cells were maintained in Roswell Park Memorial Institute (RPMI) 1640 (Sigma–Aldrich Corp., St. Louis, MO) supplemented with 1% fetal calf serum (FCS) (Hyclone Corp., Logan, UT). HuH7 cells stably overexpressing HSP20 and the control empty vector-transfected HuH7 cells were established as described previously [12], by means of a Tet-Off™ gene expression systems (Clontech Laboratories Inc., Palo Alto, CA) according to the manufacturer's instructions. The induction of HSP20 protein expression in the HSP20-overexpressing cells have been controlled by the presence of doxycycline (Sigma–Aldrich). The HSP20-overexpressing cells and the control cells were maintained in RPMI1640 supplemented with 1% FCS, 200 μg/ml G418 (Invitrogen), 100 μg/ml hygromycin B (Merck KGaA Co. Darmstadt, Germany) and 1 μg/ml doxycycline.

Tissue specimens

HCC tissues and their adjacent liver tissues were obtained by surgical resection from 35 patients in the Department of Surgery, Ogaki Municipal Hospital (Gifu, Japan), according to a protocol approved by the committee for the conduct of human research at Ogaki Municipal Hospital and at Gifu University Graduate School of Medicine. Written informed consent was obtained from all of the patients.

siRNA transfection

To knock down HSP20 in the HSP20-overexpressing HuH7 cells, the cells were transfected with a negative control siRNA or HSP20-siRNA utilizing SiLentFect according to the manufacturer's protocol. Twenty-four hours after siRNA treatment, the cells were seeded for the cell counting assay.

Cell counting assay

For cell counting, the cells were plated on 96-well dishes (3×10^3 cells/well) in RPMI1640 medium with 10% FCS without doxycycline. Twenty-four hours after seeding, the cells were treated with or without wedelolactone for 1 h, and then were stimulated with 1 nM TNF-α for the indicated periods. The cell numbers were then counted using a Cell Counting Kit-8 (Dojindo Laboratories, Kumamoto, Japan) according to the manufacturer's instructions and the Trypan blue exclusion method.

Preparation of protein samples and the Western blot analysis

In order to induce HSP20 expression, the HSP20-overexpressing cells and control cells were incubated without doxycycline for 24 h. The cells were then cultured under serum-starvation for another 24 h and subsequently treated with or without wedelolactone for 1 h, followed by stimulation with 1 nM TNF-α for the indicated periods. The cultured cells and HCC tissues were lysed, and a Western blot analysis was performed as described previously [11,12]. Briefly, sodium dodecyl sulfate–polyacrylamide gel electrophoresis (SDS–PAGE) was performed by the method described by Laemmli [15]. The proteins in the gel were transferred onto polyvinylidene fluoride (PVDF) membranes, which were then blocked with 5% fat-free dry milk in phosphate-buffered saline (PBS) with 0.1% Tween 20 for 1 h before incubation with the indicated primary antibodies. Peroxidase-labeled anti-rabbit or

anti-goat IgG antibodies were used as secondary antibodies. The peroxidase activity on the PVDF membranes was visualized on X-ray film by means of an ECL Western blotting detection system (GE Healthcare, Waukesha, WI) as described in the manufacturer's protocol. The samples from the cell cultures to be compared, and the lysates of HCC tissues and their adjacent liver tissues, which were obtained from the same patient, were run in the same gel in order to compare the protein expression levels. The data of the normalized values of the protein bands were statistically analyzed as described in the Statistical analysis section.

Densitometric analysis

The densitometric analysis was performed using a scanner and an image analysis software program (image J version 1.32). The protein levels were calculated as follows: the background-subtracted signal intensity of each protein signal was normalized to the respective GAPDH or HSP27 signal.

Real-time RT-PCR

Total RNA from the HSP20-overexpressing HuH7 cells and the control empty vector-transfected HuH7 cells was isolated and transcribed into cDNA using the Trizol reagent and an Omniscript Reverse Transcriptase kit. Real-time RT-PCR was performed using a Light Cycler system (Roche Diagnostics) in capillaries and the Fast-Start DNA Master SYBR Green I provided with the kit. Sense and antisense primers for IKK-α or GAPDH mRNA were purchased from Takara Bio Inc. (Tokyo, Japan) (primer set ID: HA034946 for IKK-α and HA067812 for GAPDH). The amplified products were determined by a melting curve analysis. The IKK-α mRNA levels were normalized to those of GAPDH mRNA.

Luciferase reporter assay

The HSP20-overexpressing HuH7 cells and the control cells were cotransfected with the *pNF-κB-luc* reporter gene (firefly luciferase; 1 μg/35-mm dish) and *pRL-CMV-luc* (*Renilla* luciferase; 100 ng/35-mm dish) using the UniFector transfection reagent (B-Bridge International, Mountain View, CA). At 8 h after transfection, the cells were stimulated by 1 nM TNF-α or vehicle for 16 h. Measurements of the luciferase activities were performed using a dual luciferase assay system (Promega Corp., Madison, WI) according to the manufacturer's instructions. Changes in the firefly luciferase activity were normalized to the changes in *Renilla* luciferase activity and the amount of total protein in the sample.

Statistical analysis

The data are expressed as the means ± SD. The statistical significance of the data was analyzed using the Mann–Whitney *U*-test. All p values were derived from two-tailed tests, and a value of $p < 0.05$ was considered to be statistically significant.

Results

Effect of HSP20-overexpression on the HuH7 cell proliferation in the presence of TNF-α

We previously demonstrated that HSP20 decreases the proliferation and increases the apoptosis of HCC cells in the absence of TNF-α [12,14]. It is firmly established that the inflammatory signaling of TNF-α contributes to HCC development [3]. In our previous study [12], we have shown that, although human HCC tissues express the HSP20 protein, HSP20 is hardly expressed in cultured HCC cells. Therefore, we have established human HCC-derived HuH7 cells which are stably transfected with wild-type HSP20 cDNA to analyze the effects of HSP20 on the TNF-α-stimulated NF-κB signaling pathway in HCC.

We first investigated the effect of the HSP20 protein on HCC cell growth under 1 nM TNF-α-induced stimulation. The growth of HSP20-overexpressing HuH7 cells was significantly suppressed compared with that in the empty vector-transfected control cells in the presence of 1 nM TNF-α (Fig. 1A). Furthermore, we found that the suppressive effects of HSP20-overexpression on the growth of HuH7 cells in the presence of 1 nM TNF-α were reversed by transfection of HSP20-siRNAs (Fig. 1B).

Suppression by HSP20-overexpression of the IKK-α protein expression in HCC cells in the absence of TNF-α

It has been shown that the NF-κB-dependent transcription is activated in response to TNF-a stimulation, which induces HCC cell proliferation [3]. It has also been shown that the growth of HuH7 cells in the presence of TNF-α is arrested by a NF-κB inhibitor, dehydroxymethylepoxyquinomicin (DHMEQ) [16]. Moreover, we found that the growth of HuH7 cells was suppressed by wedelolactone, an IKK inhibitor, in the presence of TNF-α

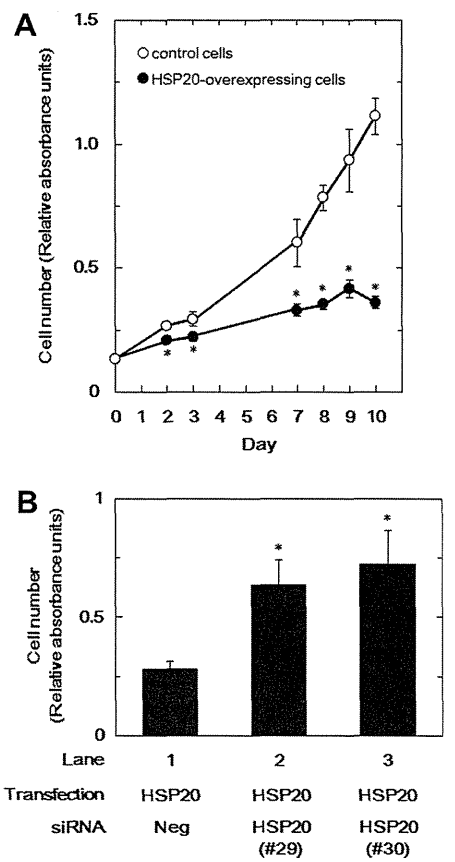

Fig. 1. The proliferation of HSP20-overexpressing HuH7 cells, and the effects of HSP20-siRNA transfection on the cell proliferation in the presence of 1 nM TNF-α. The cell growth curves of wild-type HSP20 vector-transfected HuH7 cells (HSP20-overexpressing cells: closed circles) were compared with the empty vector-transfected HuH7 cells (control cells: open circles) (A). The HSP20-overexpressing cells transfected with the negative control siRNA (Neg; lane 1) or HSP20-siRNAs (#29 and #30; lanes 2 and 3, respectively) were incubated with 1 nM TNF-α for four days (B). The data are the means ± SD ($n = 6$). *$p < 0.05$, compared to the values of the control cells (open circle) on the indicated days (A). *$p < 0.05$, compared to the value of the negative control siRNA-transfected cells (lane 1) (B).

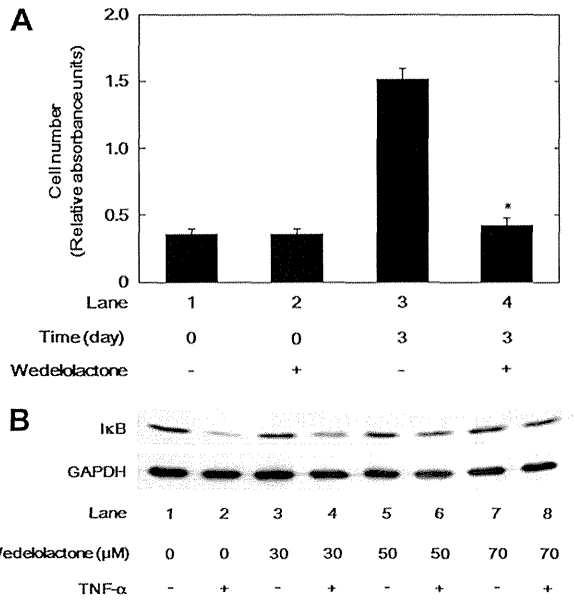

Fig. 2. The cell proliferation (A) and total IκB levels (B) of wedelolactone-treated HuH7 cells in the presence of 1 nM TNF-α. (A) The number of HuH7 cells after three days of treatment with 30 μM wedelolactone were compared with the number of control HuH7 cells without wedelolactone in the presence of 1 nM TNF-α. The values are the means ± SD ($n = 3$). *$p < 0.05$, compared to the value of cells not exposed to wedelolactone (lane 3). (B) The HuH7 cells were treated with various concentrations of wedelolactone for 1 h, then were stimulated by 1 nM TNF-α or vehicle for 20 min. The total IκB protein levels were determined by a Western blot analysis.

(Fig. 2A). Additionally, we confirmed that the IκB degradation induced by TNF-α was truly inhibited by wedelolactone in the cells (Fig. 2B). Therefore, these results indicate that TNF-α stimulates the proliferation of HuH7 cells via activation of the NF-κB pathway.

It is well recognized that the key regulatory step in the NF-κB signaling pathway involves the activation of IKK, which induces the phosphorylation of IκB and its subsequent degradation [3]. Therefore, we next investigated the protein levels of the catalytic subunits of IKK, IKK-α and IKK-β, the kinases just downstream of the TNF receptor in the NF-κB signaling pathway, in the HSP20-overexpressing HuH7 cells. As shown in Fig. 3A, the basal levels of IKK-α in the HSP20-overexpressing cells were significantly decreased in comparison with those in the control cells in the absence of TNF-α. On the other hand, the IKK-β levels did not show any difference between the HSP20-overexpressing cells and the control cells (Fig. 3B).

Effects of HSP20-overexpression on the expression levels of IKK-α mRNA in HCC cells in the absence of TNF-α

In addition, we examined the IKK-α mRNA expression levels in the HSP20-overexpressing HuH7 cells using real-time RT-PCR. As shown in Fig. 4, we found that the IKK-α mRNA expression levels in the HSP20-overexpressing HuH7 cells were significantly reduced compared with those in the control cells.

Effects of HSP20-overexpression on the IκB phosphorylation and IκB protein levels in HCC cells in the presence of TNF-α

Activated IKK phosphorylates IκB proteins and allows their ubiquitination, leading to their subsequent proteasomal degradation [3]. Therefore, we examined the effects of HSP20 on the

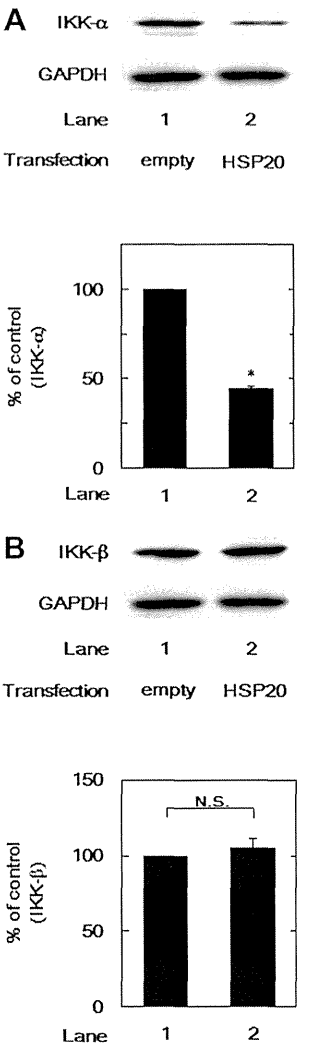

Fig. 3. The protein expression levels of IKK-α (A) and IKK-β (B) in wild-type HSP20 vector-transfected HuH7 cells (HSP20-overexpressing cells: HSP20) and empty vector-transfected HuH7 cells (control cells: empty). A Western blot analysis was performed using antibodies against IKK-α, IKK-β or GAPDH. The lower bar graph shows the quantification data for the relative protein levels of IKK-α (A) or IKK-β (B) after normalization with respect to GAPDH, as determined by a densitometric analysis. The values are the means ± SD ($n = 3$). *$p < 0.05$, compared to the value of the control cells. N.S., not significant.

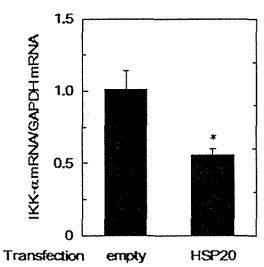

Fig. 4. The IKK-α mRNA expression levels in wild-type HSP20 vector-transfected HuH7 cells (HSP20-overexpressing cells: HSP20) and empty vector-transfected HuH7 cells (control cells: empty). The expression of IKK-α mRNA or GAPDH mRNA was quantified by real-time RT-PCR. The IKK-α mRNA levels were normalized to those of GAPDH mRNA. The values are the means ± SD ($n = 3$). *$p < 0.05$, compared to the value of the control cells.

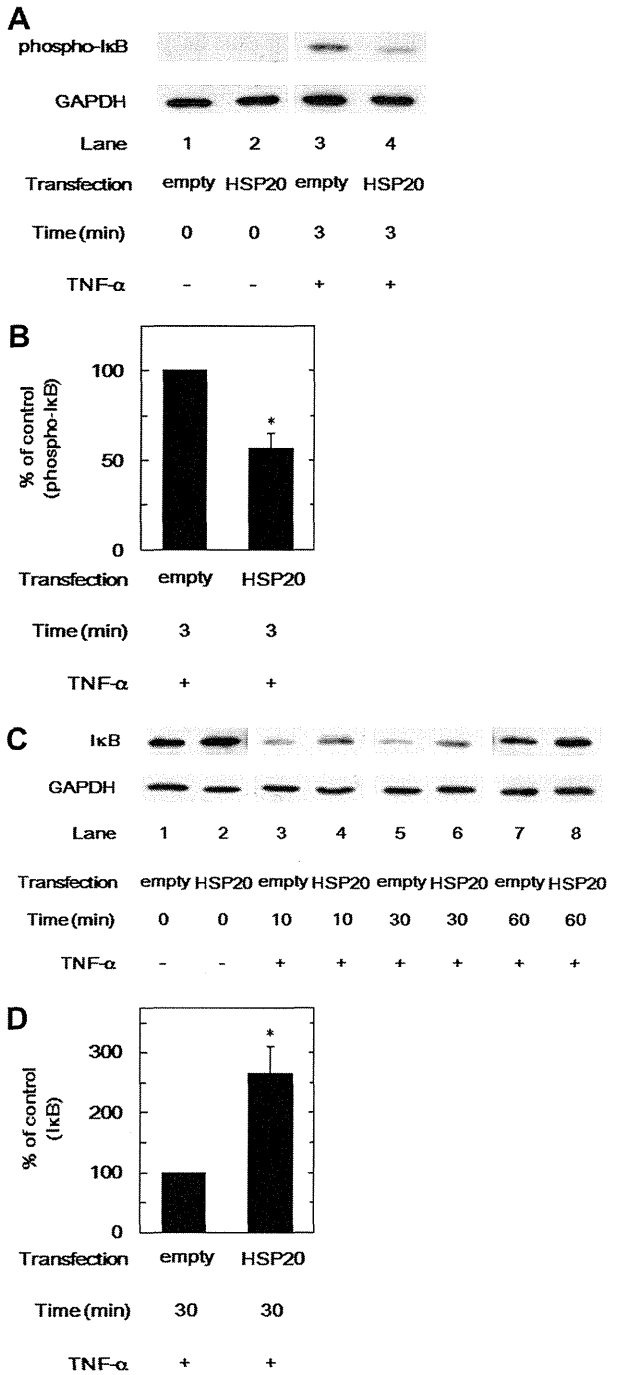

Fig. 5. The time dependent effects of TNF-α on the IκB phosphorylation and total IκB protein levels in wild-type HSP20 vector-transfected HuH7 cells (HSP20-overexpressing cells: HSP20) and empty vector-transfected HuH7 cells (control cells: empty). The HSP20-overexpressing cells or control cells were stimulated by 1 nM TNF-α for the indicated periods, and the levels of IκB phosphorylation (A) and total IκB protein (C) were determined by a Western blot analysis. The bar graphs show the quantification data for the relative levels of IκB phosphorylation at 3 min after TNF-α stimulation (B) and of the total IκB protein at 30 min after TNF-α stimulation (D). The data were normalized with respect to GAPDH, as determined by a densitometric analysis. The values are the means ± SD ($n = 3$). *$p < 0.05$, compared to the value of the control cells.

TNF-α-induced phosphorylation of IκB and the IκB protein levels in HCC cells. At the basal levels, only a little IκB phosphorylation was detected in both the HSP20-overexpressing and control cells (Fig. 5A, lanes 1 and 2). However, after TNF-α-stimulation, the phosphorylation of IκB in the HSP20-overexpressing HuH7 cells was markedly attenuated compared with that in the control cells (Fig. 5A, lane 4 in comparison with lane 3, and Fig. 5B). Accompanied by the difference in phosphorylation, decreased IκB protein levels were observed in the control cells (Fig. 5C and D). On the contrary, the protein levels of IκB in the HSP20-overexpressing cells were higher than those in the control cells (Fig. 5C and D).

Suppression by HSP20-overexpression of the NF-κB phosphorylation in HCC cells in the presence of TNF-α

The degradation of IκB liberates NF-κB, which allows it to translocate into the nucleus and exert its transcriptional activity [3]. We examined whether HSP20 expression affects the TNF-α-induced phosphorylation of NF-κB. There were not significant differences in the amount of total NF-κB protein in both the absence and the presence of TNF-α between the HSP20-overexpression cells and the control cells. On the other hand, in response to TNF-α, the phosphorylation of NF-κB in the HSP20-overexpressing cells was significantly suppressed in comparison with that in the control cells (Fig. 6A, lane 4 in comparison with lane 3, and Fig. 6B).

Suppression by HSP20-overexpression of the transactivational activity of NF-κB in HCC cells in the presence of TNF-α

The nuclear translocated NF-κB exerts its transcriptional activity by binding to NF-κB binding site on the target gene. Therefore,

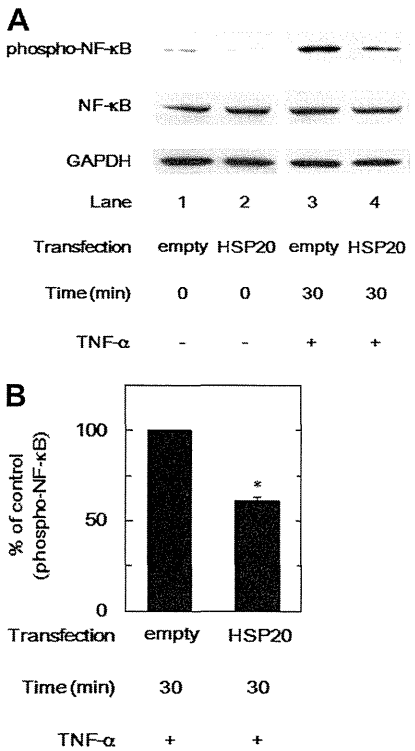

Fig. 6. The effects of TNF-α on NF-κB phosphorylation and the total NF-κB protein levels in wild-type HSP20 vector-transfected HuH7 cells (HSP20-overexpressing cells: HSP20) and empty vector-transfected HuH7 cells (control cells: empty). The HSP20-overexpressing cells or control cells were stimulated by 1 nM TNF-α for the indicated periods, and the levels of NF-κB phosphorylation and total NF-κB protein were determined by a Western blot analysis (A). The bar graph (B) shows the quantification data for the relative levels of NF-κB phosphorylation at 30 min after TNF-α stimulation. The data were normalized with respect to GAPDH, as determined by a densitometric analysis. The values are the means ± SD ($n = 3$). *$p < 0.05$, compared to the value of the control cells.

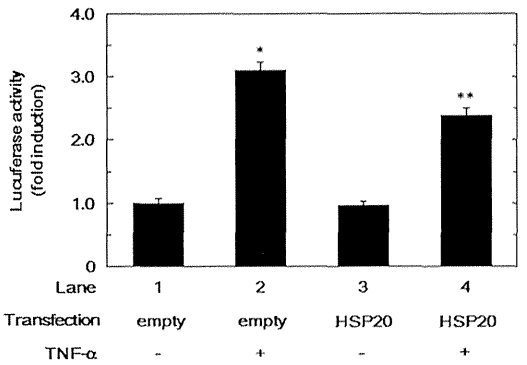

Fig. 7. The NF-κB-dependent transactivation activity in wild-type HSP20 vector-transfected HuH7 cells (HSP20-overexpressing cells: HSP20) and empty vector-transfected HuH7 cells (control cells: empty). The NF-κB-dependent transactivational activity was determined after 16 h with (lanes 2 and 4) or without (lanes 1 and 3) TNF-α stimulation. The luciferase activity in cell lysates was normalized to the *Renilla* luciferase activity and the amount of total protein. The values are the means ± SD ($n = 3$). $^{*}p < 0.05$, compared to the value of the control cells without TNF-α stimulation (lane 1); $^{**}p < 0.05$, compared to the value of the control cells with TNF-α stimulation (lane 2), and to the value of the HSP20-overexpressing cells without TNF-α stimulation (lane 3).

we performed the luciferase reporter assay using a reporter plasmid containing the luciferase reporter gene linked to NF-κB binding site. We found that although TNF-α markedly induced the luciferase activities in both the control cells and HSP20-overexpressing HuH7 cells, the luciferase activity in the HSP20-overexpressing cells was significantly lower than that in the control cells (Fig. 7).

Expression of the IKK-α protein in HCC tissues and their adjacent non-tumor tissues

We have previously reported that the expression levels of HSP20 protein in human HCC tissues were markedly lower than those in the adjacent non-tumor tissues [11]. In the present study, the IKK-α protein levels were markedly decreased in the HSP20-overexpressing HuH7 cells, as shown above (Fig. 3A). Therefore, we examined the IKK-α protein levels in surgically resected human HCC tissues and compared the results with those in the adjacent non-tumor tissues from 35 patients. The baseline characteristics of the patients with HCC are shown in Fig. 8A.

Similar to the findings in the HCC cells, the IKK-α protein levels in the human HCC tissues were significantly higher than those in

A

Gender	Male: n=26	Female: n=9		
Underlying disease	Liver cirrhosis: n=15	Chronic hepatitis: n=20		
Etiology of liver disease	HBV: n=8	HCV: n=20	Other: n=7	
Number of tumors	Solitary: n=28	Multiple: n=7		
Tumor size (mm)	<20: n=7	20-50: n=23	>50: n=5	
Vascular invasion	Negative: n=29	Positive: n=6		
Tumor stage	Stage I: n=8	Stage II: n=15	Stage III: n=12	Stage IV: n=0
Histological classification (*differentiation*)	Well: n=9	Moderately: n=25	Poorly: n=1	

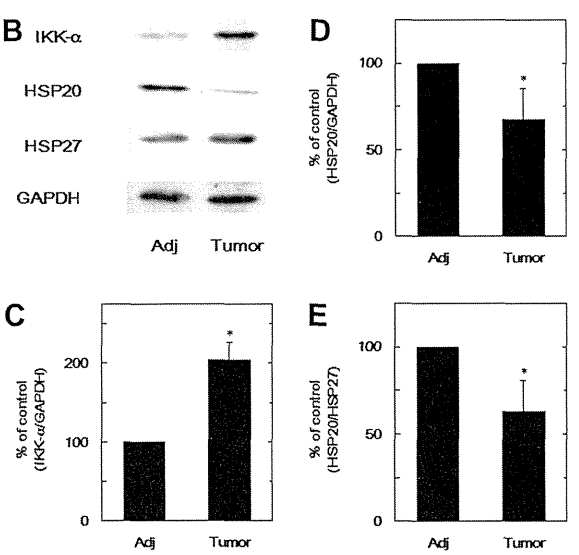

Fig. 8. The protein expression levels of IKK-α and HSP20 in human HCC tissues (Tumor) and the adjacent non-tumor liver tissues (Adj). The baseline characteristics of the patients with HCC are indicated (A). A Western blot analysis was performed using antibodies against IKK-α, HSP20, HSP27 or GAPDH (B). The bar graph shows the quantification data for the relative protein levels of IKK-α (C) and HSP20 (D) after they were normalized to the level of GAPDH, or for HSP20 (E) after it was normalized to the level of HSP27, as determined by a densitometric analysis. The data for the HCC tissues were calculated as the% ratio of the data from the respective adjacent non-tumor tissue. The values are the means ± SD ($n = 35$). $^{*}p < 0.05$, compared to the values of each adjacent non-tumor liver tissue section.

the adjacent non-tumor tissues (Fig. 8B and C and Supplementary Fig. 1). We confirmed that the expression levels of HSP20 protein in the HCC tissues are truly much lower than those in the adjacent non-tumor tissues, as has been shown in our previous study (Fig. 8B, D and E). We have also previously demonstrated that the protein levels of HSP27, another small heat shock protein, in HCC tumor tissues are not significantly different from those in the adjacent tissues (Fig. 8B) [17]. Therefore, we used the HSP27 protein as a relevant cellular epitope, and standardized the HSP20 protein expression levels in the liver tissues to the protein expression levels of GAPDH (Fig. 8D) or HSP27 (Fig. 8E) in the same tumor tissues and adjacent normal specimens.

Discussion

A persistent inflammatory reaction in the liver, which can be induced by hepatitis virus infections or chronic alcohol consumption, is closely correlated with the development of HCC [2]. The inflammatory environment helps preneoplastic hepatocytes to survive, and ultimately contributes to carcinogenesis [2,18]. TNF-α is a major inflammatory mediator in the liver, and induces the activation of IKK in hepatocytes [2,18]. Subsequently, NF-κB is activated via IKK-induced IκB phosphorylation, which is followed by its degradation, then NF-κB translocates into the nucleus, where it acts as a transcription factor [2,18]. Since regulators of proliferation, such as cyclin D1, c-Myc and cyclin E, are recognized as NF-κB target genes, TNF-α-induced NF-κB activation stimulates the growth and progression of HCC [2,18]. In the present study, we showed that the growth of HSP20-overexpresssing HuH7 cells in the presence of TNF-α was reduced compared to that of the control empty vector-transfected HuH7 cells. Moreover, HSP20-siRNA reversed the growth reduction of HSP20-overexpressing HuH7 cells in the presence of TNF-α. These findings led us to speculate that HSP20 might affect the intracellular signaling of TNF-α in HCC cells.

Therefore, we further investigated the TNF-α-stimulated IKK/IκB/NF-κB pathway in the HSP20-overexpresssing HuH7 cells compared to that in the control cells. We demonstrated that the IKK-α protein and mRNA levels were suppressed in the HSP20-overexpresssing HuH7 cells compared to those in the control cells. Based on our findings, it is possible that HSP20 might reduce the IKK-α protein levels which would result in changes in transcriptional events in the HSP20-overexpressing HCC cells. IKK is just upstream of IκB [18]. Once phosphorylated by IKK, there is immediate ubiquitin-dependent degradation of IκB by the 26S proteasome [18]. We herein demonstrated that in the presence of TNF-α, the phosphorylation of IκB and its subsequent degradation in HSP20-overexpresssing HuH7 cells were reduced compared to these findings in the control cells. In addition, the phosphorylation of Ser-536 of NF-κB following TNF-α stimulation was decreased in HSP20-overexpressing HuH7 cells.

The Ser-536 residue of NF-κB is known to be phosphorylated by TNF-α stimulation [19,20], and IKK-α reportedly phosphorylates NF-κB at Ser-536 [21]. The phosphorylation of NF-κB promotes its nuclear translocation and enhances its transactivation potential [19,22–24]. In the present study, we found the NF-κB-dependent transactivational activity induced by TNF-α in the HSP20-overexpressing HuH7 cells was significantly reduced compared to that in the control cells. It has been reported that HSP20 inhibits LPS-induced NF-κB activation in cardiomyocytes, consistent with our present results [25]. Therefore, our findings suggest that HSP20 plays a role in suppressing the NF-κB signaling pathway via the downregulation of IKK-α protein synthesis in HCC cells in the presence of TNF-α.

In our previous study [11], we have shown that the expression levels of HSP20 decrease with the progression in tumor stages in patients with HCC. Therefore, we further examined the relationship between IKK-α and HSP20 in clinical specimens from 35 patients with HCC. Compared with their adjacent non-tumor tissues, the IKK-α protein levels in human HCC specimens were truly increased. These findings suggest that the decrease in HSP20 protein expression might upregulate the IKK-α protein expression in HCC. Taking our findings into account as a whole, it is most likely that HSP20 inhibits the TNF-α-stimulated NF-κB signaling and acts as a negative regulator of HCC progression.

IKK is comprised of two catalytic (IKK-α and IKK-β) subunits and one regulatory (IKK-γ) subunit [18]. High expression levels of both IKK-α and IKK-β are closely correlated with the development of HCC [26]. It has been shown that when IKK-α and IKK-β are down-regulated in HCC cells, the numbers of BrdU positive cells are decreased, the level of apoptosis is increased and the growth of HCC is inhibited [26]. In the present study, we demonstrated that HSP20-overexpression affects the protein expression of IKK-α, but not IKK-β, in HCC.

Regarding the role of IKK-α in cancer, evidence is accumulating that activated IKK-α promotes cancer development. It has been reported that TNF-α-activated IKK-α directly phosphorylates cyclic AMP responsive element binding protein (CREB)-binding protein (CBP) in the nucleus, which induces NF-κB mediated cell proliferation and suppresses p53-dependent cell apoptosis [27,28]. In addition, interference with IKK-α activity reportedly suppresses the receptor activator of NF-κB (RANK)-induced cyclin D1 mediated proliferation of the mammary epithelium [29]. Furthermore, down-regulation of IKK-α activity has been shown to inhibit breast cancer development driven by ErB2/Her2 [18]. Based on these findings, it is probable that the down-regulation of IKK-α protein expression by HSP20 affects HCC proliferation via the TNF-α-stimulated IKK/IκB/NF-κB pathway. Our findings suggest that HSP20 represents a potential therapeutic target for HCC. Further investigations are necessary to clarify how HSP20 regulates IKK-α expression in HCC cells.

In conclusion, our results strongly suggest that HSP20 regulates TNF-α-stimulated intracellular signaling via the suppression of IKK-α expression in HCC, thus resulting in the retardation of HCC growth.

Acknowledgments

We are very grateful to Yumiko Kurokawa for her skillful technical assistance. This work was supported in part by a Grant-in-Aid for Scientific Research (25460989 to O.K.) from the Ministry of Education, Science, Sports and Culture of Japan.

Appendix A. Supplementary data

Supplementary data associated with this article can be found, in the online version, at http://dx.doi.org/10.1016/j.abb.2014.10.010.

References

[1] R.N. Aravalli, E.N.K. Cressman, C.J. Steer, Toxicology 87 (2013) 227–247.
[2] C. Berasain, J. Castillo, M.J. Perugorria, M.U. Latasa, J. Prieto, M.A. Avila, Ann. N. Y. Acad. Sci. 1155 (2009) 206–221.
[3] J.M. Schattenberg, M. Schuchmann, P.R. Galle, J. Gastroenterol. Hepatol. 26 (2011) 213–219.
[4] K. Kato, S. Goto, Y. Inaguma, K. Hasegawa, R. Morishita, T. Asano, J. Biol. Chem. 269 (1994) 15302–15309.
[5] C.M. Dreiza, P. Komalavilas, E.J. Furnish, C.R. Flynn, M.R. Sheller, C.C. Smoke, L.B. Lopes, C.M. Brophy, Cell Stress Chaperones 15 (2010) 1–11.
[6] E.V. Mymrikov, A.S. Seit-Nebi, N.B. Gusev, Physiol. Rev. 91 (2011) 1123–1159.
[7] P. Komalavilas, R.B. Penn, C.R. Flynn, J. Thresher, L.B. Lopes, E.J. Furnish, M. Guo, M.A. Pallero, J.E. Murphy-Ullrich, C.M. Brophy, Am. J. Physiol. Lung Cell. Mol. Physiol. 294 (2008) L69–L78.
[8] H.V. Edwards, R.T. Cameron, G.S. Baillie, Cell. Signal. 23 (2011) 1447–1454.
[9] H. Matsuno, O. Kozawa, M. Niwa, A. Usui, H. Ito, T. Uematsu, K. Kato, FEBS Lett. 429 (1998) 327–329.

[10] O. Kozawa, H. Matsuno, M. Niwa, D. Hatakeyama, Y. Oiso, K. Kato, T. Uematsu, Life Sci. 72 (2002) 113–124.
[11] T. Noda, T. Kumada, S. Takai, R. Matsushima-Nishiwaki, N. Yoshimi, E. Yasuda, K. Kato, H. Toyoda, Y. Kaneoka, A. Yamaguchi, O. Kozawa, Oncol. Rep. 17 (2007) 1309–1314.
[12] R. Matsushima-Nishiwaki, S. Adachi, T. Yoshioka, E. Yasuda, Y. Yamagishi, J. Matsuura, M. Muko, R. Iwamura, T. Noda, H. Toyoda, Y. Kaneoka, Y. Okano, T. Kumada, O. Kozawa, J. Cell. Biochem. 112 (2011) 3430–3439.
[13] R. Matsushima-Nishiwaki, T. Kumada, T. Nagasawa, M. Suzuki, E. Yasuda, S. Okuda, A. Maeda, Y. Kaneoka, H. Toyoda, O. Kozawa, PLoS ONE 8 (2013) e78440.
[14] T. Nagasawa, R. Matsushima-Nishiwaki, H. Toyoda, J. Matsuura, T. Kumada, O. Kozawa, Oncol. Rep. (2014), http://dx.doi.org/10.3892/or.2014.3278 [Epub ahead of print].
[15] U.K. Laemmli, Nature 227 (1970) 680–685.
[16] D. Nishimura, H. Ishikawa, K. Matsumoto, H. Shibata, Y. Motoyoshi, M. Fukuta, H. Kawashimo, T. Goto, N. Taura, T. Ichikawa, K. Hamasaki, K. Nakao, K. Umezawa, K. Eguchi, Int. J. Oncol. 29 (2006) 713–719.
[17] E. Yasuda, T. Kumada, S. Takai, A. Ishisaki, T. Noda, R. Matsushima-Nishiwaki, N. Yoshimi, K. Kato, H. Toyoda, Y. Kaneoka, A. Yamaguchi, O. Kozawa, Biochem. Biophys. Res. Commun. 337 (2005) 337–342.
[18] W.E. Naugler, M. Karin, Curr. Opin. Genet. Dev. 18 (2008) 19–26.
[19] K.J. Campbell, N.D. Perkins, Biochem. Soc. Trans. 32 (2004) 1087–1089.
[20] F. Oakley, J. Mann, S. Nailard, D.E. Smart, N. Mungalsingh, C. Constandinou, S. Ali, S.J. Wilson, H. Millward-Sadler, J.P. Iredale, D.A. Mann, Am. J. Pathol. 166 (2005) 695–708.
[21] H. Buss, A. Dörrie, M.L. Schmitz, E. Hoffmann, K. Resch, M. Kracht, J. Biol. Chem. 279 (2004) 55633–55643.
[22] R. Cui, B. Tieu, A. Recinos, R.G. Tilton, A.R. Brasier, Circ. Res. 99 (2006) 723–730.
[23] N.D. Perkins, Oncogene 25 (2006) 6717–6730.
[24] A. Moles, A.M. Sanchez, P.S. Banks, L.B. Murphy, S. Luli, L. Borthwick, A. Fisher, S. O'Reilly, J.M. van Laar, S.A. White, N.D. Perkins, A.D. Burt, D.A. Mann, F. Oakley, Hepatology 57 (2013) 817–828.
[25] X. Wang, B. Zingarelli, M. O'Connor, P. Zhang, A. Adeyemo, E.G. Kranias, Y. Wang, G.-C. Fan, J. Mol. Cell. Cardiol. 47 (2009) 382–390.
[26] R. Jiang, Y. Xia, J. Li, L. Deng, L. Zhao, J. Shi, X. Wang, B. Sun, Int. J. Cancer 126 (2010) 1263–1274.
[27] D.-F. Lee, M.-C. Hung, Clin. Cancer Res. 14 (2008) 5656–5662.
[28] A. Chariot, Trends Cell Biol. 19 (2009) 404–413.
[29] M. Karin, Y. Cao, F.R. Greten, Z.-W. Li, Nat. Rev. Cancer (2002) 301–310.

Hepatol Int (2015) 9:84–92
DOI 10.1007/s12072-014-9553-5

ORIGINAL ARTICLE

Non-hypervascular hypointense nodules on Gd-EOB-DTPA-enhanced MRI as a predictor of outcomes for early-stage HCC

Hidenori Toyoda · Takashi Kumada · Toshifumi Tada · Yasuhiro Sone · Atsuyuki Maeda · Yuji Kaneoka

Received: 17 March 2014 / Accepted: 21 June 2014 / Published online: 23 July 2014

Abstract
Background/purpose In patients with hepatocellular carcinoma (HCC), gadolinium-ethoxybenzyl-diethylenetriamine pentaacetic acid (Gd-EOB-DTPA)-enhanced magnetic resonance imaging (MRI) often identifies non-hypervascular hypointense hepatic nodules during the hepatobiliary phase, but their prognostic significance is unclear. We conducted a prospective observational study to investigate the impact of non-hypervascular hypointense hepatic nodules detected by Gd-EOB-DTPA-enhanced MRI on the outcome of patients with early-stage HCC.
Methods Post-treatment recurrence and survival rates were analyzed in 138 patients with non-recurrent, early-stage HCC [Barcelona Clinic Liver Cancer (BCLC) stage 0 or A] and Child-Pugh A liver function according to the presence of non-hypervascular hypointense nodules on pretreatment Gd-EOB-DTPA-enhanced MRI.
Results Non-hypervascular hypointense hepatic nodules were detected in 51 (37.0 %) patients with early-stage HCC on pretreatment Gd-EOB-DTPA-enhanced MRI. Recurrence rates were significantly higher in patients with non-hypervascular hypointense nodules ($p < 0.0001$). Based on a multivariate analysis, the presence of non-hypervascular hypointense hepatic nodules on Gd-EOB-DTPA-enhanced MRI was independently associated with an increased recurrence rate, independent of tumor progression or treatment ($p = 0.0005$). The survival rate was significantly lower in patients with non-hypervascular hypointense nodules on Gd-EOB-DTPA-enhanced MRI ($p = 0.0108$).
Conclusions In patients with early-stage typical HCC (BCLC 0 or A), the presence of concurrent non-hypervascular hypointense hepatic nodules in the hepatobiliary phase of pretreatment Gd-EOB-DTPA-enhanced MRI is an indicator of higher likelihood of recurrence after treatment and may be a marker for unfavorable outcome.

Keywords Hepatocellular carcinoma · Early stage · Gd-EOB-DTPA-enhanced MRI · Non-hypervascular hypointense nodules · Recurrence · Survival

Abbreviations

Gd-EOB-DTPA	Gadolinium-ethoxybenzyl-diethylenetriamine pentaacetic acid
MRI	Magnetic resonance imaging
HCC	Hepatocellular carcinoma
US	Ultrasonography
MDCT	Multidetector-row computed tomography
BCLC	Barcelona Clinic Liver Cancer
AASLD	American Association for the Study of Liver Diseases
RFA	Radiofrequency ablation
AFP	Alpha-fetoprotein
AFP-L3	*Lens culinaris* agglutinin-reactive alpha-fetoprotein

Electronic supplementary material The online version of this article (doi:10.1007/s12072-014-9553-5) contains supplementary material, which is available to authorized users.

H. Toyoda (✉) · T. Kumada · T. Tada
Department of Gastroenterology, Ogaki Municipal Hospital, 4-86 Minaminokawa, Ogaki, Gifu 503-8502, Japan
e-mail: hmtoyoda@spice.ocn.ne.jp

Y. Sone
Department of Radiology, Ogaki Municipal Hospital, Ogaki, Japan

A. Maeda · Y. Kaneoka
Department of Surgery, Ogaki Municipal Hospital, Ogaki, Japan

DCP	Des-gamma-carboxy prothrombin
CTHA	CT during hepatic arteriography
TACE	Transarterial chemoembolization
ALT	Alanine amonotransferase activity

Introduction

Hepatocellular carcinoma (HCC) is one of the most common cancers and causes of cancer-related death worldwide [1]. Tremendous efforts have been made for the detection of hepatic nodules including early-stage HCC, improving various imaging techniques including ultrasonography (US), multidetector-row computed tomography (MDCT), and magnetic resonance imaging (MRI).

The liver-specific contrast agent gadolinium-ethoxybenzyl-diethylenetriamine pentaacetic acid (Gd-EOB-DTPA), which is taken up by hepatocytes, has been in clinical use for dynamic MRI studies since February 2008 in Japan. Gd-EOB-DTPA provides both dynamic and liver-specific hepatobiliary MR images [2–5]. In the hepatobiliary phase image, hepatic lesions that lack normally functioning hepatocytes are visualized as an absence of hepatocyte-selective enhancement compared to normal parenchyma [5, 6]. The use of Gd-EOB-DTPA-enhanced MRI increases detection of concurrent non-hypervascular hepatic nodules, which appear as hypointense nodules during the hepatobiliary phase, in patients with HCC. It is controversial whether the presence of these non-hypervascular hepatic nodules in patients with typical hypervascular HCC lesions impacts their outcome after treatment for HCC.

In the present study, we attempted to evaluate the impact of concurrent non-hypervascular hepatic nodules detected as hypointense nodules during the hepatobiliary phase of Gd-EOB-DTPA-enhanced MRI on recurrence and survival of patients with early-stage HCC.

Methods

Patients, treatment, and follow-up

A total of 374 patients were diagnosed with primary, non-recurrent HCC between February 2008 and March 2013 at our institution. Of these patients, 289 underwent Gd-EOB-DTPA-enhanced MRI within 2 weeks prior to treatment, and 212 of 289 patients had Child-Pugh class A [7] liver function. Based on the Barcelona Clinic Liver Cancer (BCLC) classification, 138 of 212 patients were classified as early-stage HCC (stage 0 or A) [8]. The diagnosis of HCC was based on appropriate imaging characteristics according to criteria in the guidelines of the American Association for the Study of Liver Diseases (AASLD) [9, 10]. Decisions regarding treatment for each individual patient were based on Japanese treatment guidelines for HCC [11]. Pretreatment Gd-EOB-DTPA-enhanced MRI image findings had not been taken into consideration in the selection of treatment option. All patients were treated by hepatic resection or radiofrequency ablation (RFA). In patients who underwent hepatic resection, HCC tumors were resected with ample margins; enucleation of tumors without margins was not performed. In patients who underwent RFA, HCC were confirmed to be ablated by dynamic CT within a week after RFA. Multiple ablations were performed by repeated RFA sessions when enough ablation of HCC tumor with ample margins was not achieved.

After treatment, all patients were prospectively followed until the end of November 2013 at our institution with US and either MDCT or MRI every 3–6 months. Regular monitoring of serum tumor markers [alpha-fetoprotein (AFP), *lens culinaris* agglutinin-reactive alpha-fetoprotein (AFP-L3), and des-gamma-carboxy prothrombin (DCP)] was performed every 3 months. When a suspicious hepatic nodule was detected by US or an elevation in tumor markers was observed, additional imaging (usually MDCT or MRI) was performed to check for HCC recurrence. Recurrence was diagnosed by appropriate imaging characteristics according to criteria in the AASLD guidelines [9, 10]. It was confirmed by pathologic examination of resected specimens when patients underwent repeated hepatic resection. Recurrent HCC was categorized into two groups prior to the study as intrahepatic metastasis or multicentric recurrence according to a previous study [12, 13]. Intrahepatic metastasis was defined as recurrent tumors consisting of moderately or poorly differentiated HCC with the same or lower degree of differentiation than the primary tumors on pathologic examination or hypervascular tumor without non-hypervascular peripheral regions in a same hepatic segment on imaging examination. Multicentric recurrence was defined according to previously reported criteria with some modifications [14, 15] as follows: (i) the recurrent tumor consists of well-differentiated HCC occurring in a different hepatic segment than moderately or poorly differentiated pre-existing HCCs; (ii) both the primary and recurrent tumors are well-differentiated HCCs; and (iii) the recurrent tumor contained regions of dysplastic nodules in peripheral areas based on pathologic examination or contained non-hypervascular regions in peripheral areas of hypervascular tumor on imaging examination.

Pretreatment imaging examination of liver nodules using Gd-EOB-DTPA-enhanced MRI and confirmation of non-hypervascular hypointense hepatic nodules

All patients underwent Gd-EOB-DTPA-enhanced MRI within 2 weeks of treatment. MRI was performed using a 1.5-T whole-body MRI system (Intera Achieva 1.5T NOVA; Philips Medical Systems, Tokyo, Japan) with a phased-array body coil as the receiver coil. T1-weighted sequences were acquired with the following parameters: T1-weighted turbo field echo (TFE) in-phase and opposed-phase transverse (TE, opposed-phase 2.3 ms, in-phase 4.6 ms; flip angle, 12°; matrix size, 320 × 512; scan percentage, 70) with 3.5-mm section thickness, a 0-mm intersection gap, and a 38-cm field of view. After intravenous injection of Gd-EOB-DTPA (Primovist; Bayer Schering Pharma, Osaka, Japan), T1-weighted transverse gradient-echo sequences [high-resolution isotropic volume examination (THRIVE) with spectral presaturation inversion recovery (SPIR), 4/1.8; flip angle, 12°; matrix size, 320 × 512; scan percentage, 78.54] with 3.5-mm section thickness, a 0-mm intersection gap, and a 38-cm field of view were obtained. Gd-EOB-DTPA was administered intravenously as a bolus at a rate of 2 mL/sec (0.1 mL/kg, maximum dose of 10 mL) through an intravenous antecubital line (20–22 gauge), which was flushed with 20 mL of saline using a power injector (Sonic Shot; Nemoto Kyorindo, Tokyo, Japan). The timing for dynamic arterial phase imaging was determined using MR fluoroscopic bolus detection in the descending aorta (Bolus Trak; Philips Medical Systems). The mean delay times (time interval between the start of bolus administration and the start of image acquisition) for the arterial, portal, and transitional phases were 20, 60, and 180 s, respectively. Immediately after the dynamic study, a respiration-triggered single-shot T2-weighted sequence with a reduction factor of 4 (1,200/100; flip angle, 90°; matrix size, 400 × 512) with 7-mm section thickness, a 1-mm intersection gap, and a 38-cm field of view was obtained with SPIR. The hepatobiliary phase [16] was obtained after a 20-min delay with a T1-weighted TFE sequence (TR/TE, 4.3/2.1 ms; flip angle, 12°; matrix size, 288 × 512) with 3.5-mm section thickness, a 0-mm intersection gap, and a 38-cm field of view. All the sequences were obtained with parallel imaging (SENSE). Hypointense hepatic nodules detected during the hepatobiliary phase of Gd-EOB-DTPA-enhanced MRI were low-intensity nodules greater than 3.5 mm.

Prior to treatment, all patients underwent dynamic CT and CT during hepatic arteriography (CTHA) [17–19] to evaluate the intranodular blood supply and to confirm the hypervascularity of HCC lesions and the lack of hypervascularity of non-hypervascular hepatic nodules.

All imaging findings were independently evaluated by a radiologist (Y.S.) and a hepatologist (H.T.) who were blinded to the clinical data. When imaging assessments between the two reviewers were discordant, consensus was achieved through discussion.

Assays of AFP and DCP

Pretreatment tumor marker levels were measured within 1 week of treatment. Serum AFP were measured using microchip capillary electrophoresis and a liquid-phase binding assay on a μTASWako i30 auto-analyzer (Wako Pure Chemical Industries, Ltd., Osaka, Japan) [20]. Serum DCP levels were determined using a sensitive enzyme immunoassay (Eitest PIVKA-II kit, Eisai Laboratory, Tokyo, Japan) [21–23]. The cut-off value of 20 ng/mL was used to establish positivity for AFP, as proposed by Oka et al. and Koda et al. [24, 25]. The cut-off value used to establish positivity for DCP was 40 mAU/mL, as proposed by Okuda et al. [26].

Statistical analyses

Differences in percentages between groups were analyzed using the chi-square test. Differences in mean quantitative values were analysed using the Mann–Whitney *U* test. The date of treatment for HCC was defined as time zero for calculations of overall survival and recurrence rates. In the analysis of overall survival rates, patients who were alive were censored, and those who died were not censored. In the analysis of recurrence rates patients without HCC recurrence were censored, and patients who had died or had HCC recurrence were not censored. The Kaplan–Meier method [27] was used to calculate survival and recurrence rates, and the log-rank test [28] was used to analyze differences.

The Cox proportional hazards model [29] was used for univariate and multivariate analyses of factors related to overall survival and recurrence rates. Variables analyzed included patient age and sex, alanine aminotransferase activity (ALT), platelet count, tumor size (≤2 cm/between 2 and 3 cm), number of tumors (single/multiple), pretreatment AFP level (≤20/>20 ng/dL), pretreatment DCP level (≤40/>40 mAU/mL), treatment for HCC (hepatectomy/RFA), and presence of non-hypervascular hypointense nodules in the hepatobiliary phase of Gd-EOB-DTPA-enhanced MRI (absent/present). Variables that reached statistical significance ($p < 0.05$) in the univariate analysis were subsequently included in the multivariate analysis. Data analyses were performed

Table 1 Characteristics of the study patients ($n = 138$)

Characteristic	Value
Age (mean ± SD, years) (range)	70.6 ± 9.2 (36–85)
Sex (female/male)	41 (29.7)/97 (70.3)
Etiology (HBV/HCV/non-HBV, non-HCV)	24 (17.4)/95 (68.8)/19 (13.8)
Alanine aminotransferase (IU/L)	46.5 ± 31.0
Albumin (mean ± SD, g/dL)	3.93 ± 0.42
Total bilirubin (mean ± SD, mg/dL)	0.84 ± 0.32
15-min ICG retention rate (%)	18.8 ± 10.2
Prothrombin (%)	89.8 ± 14.2
Platelet count (×1,000/mL)	144 ± 67
Tumor size (mean ± SD, cm) (range)	1.93 ± 0.61 (0.7–3.0)
Number of tumors (single/multiple)	105 (76.1)/33 (23.9)
BCLC classification (stage 0/stage A)	63 (45.7)/75 (54.3)
AFP (ng/dL) (median, range)	11.4 (0.6–3,344)
DCP (mAU/mL) (median, range)	29.0 (0–25,763)
Non-hypervascular hypointense nodule (absent/present)	87 (63.0)/51 (37.0)
Treatment (resection/radiofrequency ablation)	76 (55.1)/62 (44.9)
Follow-up period (months) (median, range)	33.1 (8.2–66.4)

Percentages are given in parentheses as appropriate

HBV hepatitis B virus, *HCV* hepatitis C virus, *ICG* indocyanine green test, *BCLC* Barcelona Clinic Liver Cancer group, *AFP* alpha-fetoprotein, *DCP* des-gamma-carboxy prothrombin

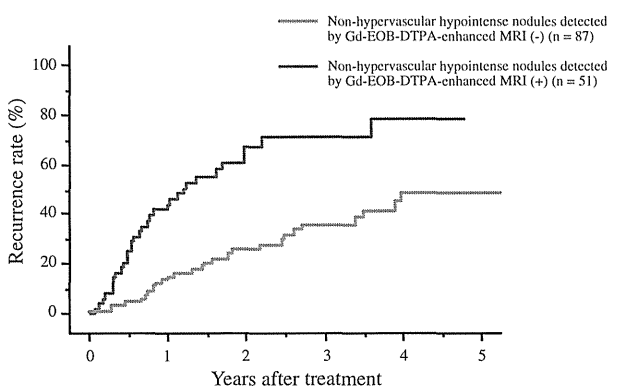

Fig. 1 Recurrence rates after treatment in patients with early-stage hepatocellular carcinoma (Barcelona Clinic Liver Cancer stage 0 or A) based on the presence or absence of non-hypervascular hypointense hepatic nodules identified during the hepatobiliary phase of gadolinium-ethoxybenzyl-diethylenetriamine pentaacetic acid (Gd-EOB-DTPA)-enhanced MRI. The recurrence rate was significantly higher in patients with non-hypervascular hypointense hepatic nodules on Gd-EOB-DTPA-enhanced MRI than patients without such lesions ($p < 0.0001$)

using JMP statistical software, version 6.0 (Macintosh version; SAS Institute, Cary, NC, USA). All p values were derived from 2-tailed tests, with $p < 0.05$ accepted as statistically significant.

Results

Patients characteristics

Table 1 shows the characteristics of the study patients. Patients consisted of 97 males and 41 females, with a mean age of 70.6 ± 9.2 years. There were 63 (37.3 %) patients with BCLC stage 0 HCC [8]. HCC was treated with hepatic resection in 76 (55.1 %) patients and RFA in the remaining 62 (44.9 %) patients. In patients treated by RFA, transarterial chemoembolization (TACE) was performed before RFA in patients whose HCC was more than 2.0 cm in diameter, in order to enhance the efficacy of RFA [30], and 29 (46.8 %) of the 62 patients underwent TACE before RFA. No differences in both recurrence and survival rates were observed between patients treated by RFA with and without TACE ($p = 0.6295$ for recurrence and $p = 0.4256$ for survival; supplementary Fig. 1).

Non-hypervascular hypointense nodules were detected on pretreatment Gd-EOB-DTPA-enhanced MRI in 51 (37.0 %) patients, who were categorized as the hypointense nodule (+) group. The other 87 (63.0 %) patients in whom non-hypervascular hypointense nodules were not detected were classified into the hypointense nodule (−) group. Patients were followed for 8.2–66.4 months (median follow-up, 33.1 months) after treatment.

Recurrence rates after treatment according to the presence of non-hypervascular hypointense nodules detected during pretreatment Gd-EOB-DTPA-enhanced MRI

Recurrence of HCC was observed in 60 (43.5 %) of 138 patients during the study period. Recurrence was diagnosed based on appropriate imaging characteristics according to criteria in the AASLD guidelines in all patients and, in addition, it was confirmed by pathologic examination of resected specimens in 12 patients who underwent hepatic resection for recurrent HCC.

Recurrence of HCC was observed in 32 patients (62.7 %) of the hypointense nodule (+) group and 28 patients (32.2 %) of the hypointense nodule (−) group. We determined the recurrence rate after treatment based on the presence or absence of non-hypervascular hypointense hepatic nodules identified during the hepatobiliary phase of Gd-EOB-DTPA-enhanced MRI (Fig. 1). The recurrence rate was significantly higher in patients in the hypointense nodule (+) group than patients in the hypointense nodule (−) group ($p < 0.0001$). In the univariate analysis, elevation of ALT ($p = 0.0282$), multiple tumors ($p = 0.0035$), pretreatment elevation of serum AFP level ($p = 0.0491$), RFA ($p = 0.0087$), and the presence of non-hypervascular hypointense nodules on pretreatment Gd-EOB-DTPA-